Journal of Magnetic Resonance 203 (2010) 29–43

Contents lists available at ScienceDirect

Journal of Magnetic Resonance

journal homepage: www.elsevier.com/locate/jmr

Theoretical analysis of the sensitivity of dipolar field signal to local field variations by perturbative expansion of the magnetization

Chung Ki Wong

CPU Box 276852, Rochester, NY 14627-6852, USA

ARTICLE INFO

Article history:
Received 10 July 2009
Revised 24 November 2009
Available online 29 November 2009

Keywords:
Distant dipolar field (DDF)
Intermolecular multiple-quantum coherence (iMQC)
Susceptibility-induced field
Sub-voxel field variation

ABSTRACT

A perturbation method based on the integral form of the Bloch equation is used to calculate the distant dipolar field (DDF) signal formed by the correlation spectroscopy revamped by asymmetric *z*-gradient echo detection (CRAZED) sequence in the presence of a susceptibility-induced field. The properties of the DDF signal are analyzed through the series expansion of the magnetization, and the first order DDF result is applied to study the use of the DDF effect to probe sub-voxel field distributions. Numerical calculations are carried out with the sub-voxel field distributions modeled by rectangular tubes of uniform frequency shifts (the block model) and cylinders of a finite susceptibility difference (the blood vessel model) using the parameters for brain at 9.4 T. The DDF signal is found to exhibit features arising from the sub-voxel structures.

1. Introduction

Over the past two decades, there has been an increasing interest in studying the magnetic resonance (MR) signals of liquids formed under the influence of distant dipolar field (DDF). In the presence of a linear gradient field, the DDF experienced by a spin is found to be contributed predominantly from the surrounding magnetization of the spin within a correlation length, which is defined as half of the spatial modulation period induced by the gradient field [1]. It is thus suggested that, by varying this modulation period, the magnetization distribution can be probed with the use of the DDF effect [2]. The specific sensitivity of the DDF signal to the user-defined distance may therefore provide a new contrast mechanism for MR imaging that is able to assess sample structures in vivo on a sub-voxel length scale.

The use of the DDF effect on MR image contrast has been explored in the studies of tumors [3,4], brains [5,6], functional magnetic resonance imaging (fMRI) [7–10], and structural anisotropy [11]. In particular, the dependence of the DDF signal on the correlation length have been examined in the structural studies using phantoms [12–24], trabecular bones [25–28], and fMRI [29]. In the studies of the sample structures arising from spin density distribution (i.e., the equilibrium magnetization distribution), the DDF signal was found to be able to reveal the length scales of the structures as the correlation distance is varied [12–14,17–19,22,24]. Nevertheless, for the applications in fMRI, oncological and other in vivo studies, the magnetic field is perturbed on a length scale determined by the local structures due to the electronic susceptibility mismatches arising, for example, between blood and the surrounding tissue. In these cases, it is the suggested sensitivity of the DDF signal to the sub-voxel variations of the susceptibility-induced field on a specific length scale that would be more important.

Experiments and numerical simulations have been done to explore the sensitivity of the DDF signal to the variations of the magnetic field on a specific length scale [15,16,20,21,23,28,29]. While earlier works suggested that there is a change in the DDF signal when the correlation distance is close to a particular length scale of the field variation [15,16], more recent studies were not able to confirm such a relation [20,21,23,28,29]. In addition, these works primarily describe the phenomena from the results instead of providing rigorous explanations. Therefore analytical works are needed to truly understand the extendability of the sensitivity of the DDF signal to local field variations induced by susceptibility inhomogeneities.

In this paper, the dependence of the DDF signal on the correlation length and the properties of the local field variations is studied analytically and numerically. A simplified model that has a uniform spin density distribution is considered, so that all structural effects come solely from the local field variations. This approach helps us to investigate whether the suggested sensitivity of the DDF signal to the characteristic length scales of the sub-voxel field variations, such as the variation length scales of the susceptibility-induced fields introduced by blood vessels, can be observed.

The work of this paper begins in Section 2 by rewriting the Bloch equation in an integral form. The magnetization is then expanded as a series in different orders of the DDF effect. From the series expansion, certain general properties of the DDF signal are

E-mail address: ckwong@pas.rochester.edu

1090-7807/$ - see front matter © 2009 Elsevier Inc. All rights reserved.
doi:10.1016/j.jmr.2009.11.018

observed. In Section 3, the first order solution of the magnetization is applied to the correlation spectroscopy revamped by asymmetric z-gradient echo detection (CRAZED) sequence [1]. The result is written in k-space, which simplifies the nonlocal dependence of the spatial integral of the dipolar field on the relative spin positions. It is then used in Section 4 to study the sensitivity of the DDF signal to sub-voxel susceptibility-induced field variations. Numerical calculations of the DDF signal are carried out using the block model (blocks of uniform resonance frequency shifts) and the blood vessel model (infinitely long cylinders with a finite susceptibility difference). Finally, the results and their implications are summarized in Section 5.

The results presented in this paper are based on the works in Chapter 6 of Ref. [30].

2. Perturbative expansion of the magnetization in dipolar field

In this section, the evolution of the magnetization is considered for general distributions of the spin density and the susceptibility-induced field under the influence of the distant dipolar field. To probe the spatial distribution of the susceptibility-induced field using the DDF effect, the correlation distance induced by the gradient fields is required to be the same order of magnitude as the spatial variation of the magnetization. In this case, the magnetization cannot be treated as uniform nor highly modulated by the gradient field [31–33]. Because of the nonlocal spatial dependence of the DDF, the system has to be treated as a nonlocal problem.

To proceed, we express the Bloch equation in an integral form, and consider a perturbative expansion of the magnetization in powers of the dipolar field. Similar approach of using the DDF effect as a perturbation factor in solving the Bloch equation has been used previously in studying the DDF signal behavior [12,13,17,18,34–36]. The perturbative method was found to be in good agreement with the full numerical calculations and the experiments when the pulse sequence time is not too long. The theory developed in this paper extends the previous works to include explicitly the susceptibility-induced field.

2.1. Nonlinear integral form of the Bloch equation

In the rotating frame, the Bloch equation during free evolution is written as

$$\frac{\partial M_z(\vec{r},t)}{\partial t} = \frac{i\gamma}{2}[B_{d-}(\vec{r},t)M_+(\vec{r},t) - B_{d+}(\vec{r},t)M_-(\vec{r},t)], \tag{1a}$$

$$\frac{\partial M_\pm(\vec{r},t)}{\partial t} = \pm i\gamma B_{d\pm}(\vec{r},t)M_z(\vec{r},t) + \left\{\mp i[\Delta\omega(\vec{r}) + \gamma B_{dz}(\vec{r},t)] - \frac{1}{T_2}\right\}M_\pm(\vec{r},t), \tag{1b}$$

where γ is the gyromagnetic ratio, $\vec{M}$ is the magnetization, T_2 is the transverse relaxation time, $\vec{B}_d$ is the distant dipolar field, and $\Delta\omega(\vec{r})$ is the distribution of the resonance frequency offset due to the susceptibility-induced magnetic field. The transverse components of the dipolar field and the magnetization are, respectively, given by

$$B_{d\pm}(\vec{r},t) = B_{dx}(\vec{r},t) \pm iB_{dy}(\vec{r},t), \tag{2a}$$

$$M_\pm(\vec{r},t) = M_x(\vec{r},t) \pm iM_y(\vec{r},t). \tag{2b}$$

Since $M_x(\vec{r},t)$ and $M_y(\vec{r},t)$ are real quantities, $M_+(\vec{r},t)$ and $M_-(\vec{r},t)$ are complex conjugates of each other, i.e., $M_+(\vec{r},t) = [M_-(\vec{r},t)]^*$. Likewise, $B_{d+}(\vec{r},t) = [B_{d-}(\vec{r},t)]^*$.

In writing Eq. (1), the effects of the longitudinal relaxation and diffusion on the magnetization evolution are ignored for simplicity.To acquire maximal DDF signal, the evolution period of the pulse sequence is taken to be the same order of magnitude as the transverse relaxation time (T_2), which is usually much shorter than the longitudinal relaxation time (T_1) for most biological tissues. On the other hand, in Fourier space, free diffusion causes the component of the magnetization with wave vector $\vec{k}_m$ to decay as $\exp(-Dk_m^2 t)$, where D is the diffusion coefficient. The time scale for such a decay is about $\tau_D = (Dk_m^2)^{-1}$. The diffusion coefficient for water in tissues at room temperature is $D \simeq 10^{-9}\ \mathrm{m^2 s^{-1}}$. For a modulation with wave vector $k_m \simeq 20\ \mathrm{mm^{-1}}$, the decay time due to diffusion is about 2.5 s, which is much longer than the transverse relaxation time of most biological tissues. As a result, both T_1 relaxation and diffusion can be safely neglected in the Bloch equation.

For general distributions of the spin density and the susceptibility-induced field, the localized form for the dipolar field in position space [31–33] is no longer valid. The general form of the distant dipolar field is given by [31]

$$\vec{B}_d(\vec{r},t) = \frac{\mu_0}{4\pi}\int_S d^3\vec{r}'\ T(\vec{r}-\vec{r}')\left[3\left(\vec{M}(\vec{r}',t)\cdot\hat{z}\right)\hat{z} - \vec{M}(\vec{r}',t)\right], \tag{3}$$

where μ_0 is the permeability of vacuum, $\int_S d^3\vec{r}'$ denotes the integration over the sample volume,

$$T(\vec{r}-\vec{r}') = \frac{3\cos^2\theta_{\vec{r}\vec{r}'} - 1}{2|\vec{r}-\vec{r}'|^3} \tag{4}$$

is the dipolar field factor, and $\theta_{\vec{r}\vec{r}'}$ is the angle between the vector $(\vec{r}-\vec{r}')$ and the z-axis. The Fourier transform of the dipolar field factor is given by

$$\widetilde{T}(\vec{k}) \equiv \frac{1}{(2\pi)^3}\int d^3\vec{u}\, e^{-i\vec{k}\cdot\vec{u}}T(\vec{u}) = -\frac{4\pi}{3}\frac{1}{(2\pi)^3}\left[\frac{3(\hat{k}\cdot\hat{z})^2 - 1}{2}\right]. \tag{5}$$

It should be noted that the Fourier transform of the dipolar field factor $\widetilde{T}(\vec{k})$ depends only on the angle between the vector $\vec{k}$ and the z-axis, i.e.,

$$\widetilde{T}(\vec{k}) = \widetilde{T}(\hat{k}) = \widetilde{T}(-\vec{k}). \tag{6}$$

Using the notation of the dipolar field factor, Eq. (1) can be written as two coupled nonlinear integral equations:

$$M_z(\vec{r},t) = M_z(\vec{r},t_0) - \frac{i\gamma\mu_0}{8\pi}\int_{t_0}^{t}dt'\int d^3\vec{r}'[M_+(\vec{r},t')T(\vec{r}-\vec{r}')M_-(\vec{r}',t') - M_-(\vec{r},t')T(\vec{r}-\vec{r}')M_+(\vec{r}',t')], \tag{7a}$$

$$M_\pm(\vec{r},t) = M_\pm(\vec{r},t_0)e^{\left[\mp i\Delta\omega(\vec{r})-\frac{1}{T_2}\right](t-t_0)} \mp \frac{i\gamma\mu_0}{4\pi}\int_{t_0}^{t}dt' \times \int d^3\vec{r}'\, e^{\left[\mp i\Delta\omega(\vec{r})-\frac{1}{T_2}\right](t-t')}[2M_\pm(\vec{r},t')T(\vec{r}-\vec{r}')M_z(\vec{r}',t') + M_z(\vec{r},t')T(\vec{r}-\vec{r}')M_\pm(\vec{r}',t')], \tag{7b}$$

where $\vec{M}(\vec{r},t_0)$ is the initial magnetization at time t_0. Note that Eq. (7) is the integral form (not the solution) of Eq. (1). The spatial integrals on the right hand side of Eq. (7) exhibit the nonlinear couplings of the magnetization $\vec{M}(\vec{r},t')$ with itself $\vec{M}(\vec{r}',t')$ through the dipolar field factor $T(\vec{r}-\vec{r}')$. Since $\vec{M}(\vec{r}',t')$ also depends on the magnetization at other positions and so forth, the integrals are infinite series in the dipolar field interactions, with the number of dipolar field interactions in each term of the series equal to the number of the dipolar field factors.

By substituting $M_z(\vec{r},t)$ and $M_\pm(\vec{r},t)$ back to the right hand side of Eq. (7), the magnetization can be written as a series:

$$\vec{M}(\vec{r},t) = \vec{M}^{(0)}(\vec{r},t) + \vec{M}^{(1)}(\vec{r},t) + \vec{M}^{(2)}(\vec{r},t) + \cdots, \tag{8}$$

where $\vec{M}^{(n)}$ is the nth order dipolar field term of the magnetization, which is proportional to the product of n dipolar field factors T and $n+1$ initial magnetizations $M_i(\vec{r},t_0)$ with $i=z$ or $\pm$. The zeroth order term $\vec{M}^{(0)}(\vec{r},t)$ in Eq. (8) is the solution of Eq. (1) in the absence of the dipolar field, whereas the high order terms provide indications about the order of magnitude of deviations from the zeroth order approximation due to the DDF effect.

It is noted that the DDF interaction is a small effect in most biological tissues. Each successive term of Eq. (8) is typically smaller than the previous term by roughly the product of the dipolar frequency ($\gamma\mu_0 M_0$) and the duration of the pulse sequence, where M_0 is the equilibrium magnetization. Therefore only the first few terms are important in the calculation of the DDF signal. For instance, the zeroth order approximation of the magnetization can be obtained by solving Eq. (1) in the absence of the dipolar field, which is given by

$$M_z^{(0)}(\vec{r},t) = M_z(\vec{r},t_0), \tag{9a}$$

$$M_\pm^{(0)}(\vec{r},t) = M_\pm(\vec{r},t_0)e^{\left[\mp i\Delta\omega(\vec{r})-\frac{1}{T_2}\right](t-t_0)}. \tag{9b}$$

By iterating Eq. (7) to the first order of the DDF, the first order term is found to be

$$\begin{aligned} M_z^{(1)}(\vec{r},t) = &-\frac{i\gamma\mu_0}{8\pi}\int_{t_0}^{t} dt'\, e^{-\frac{2(t'-t_0)}{T_2}}\int d^3\vec{r}'\; T(\vec{r}-\vec{r}') \\ &\times\Big[M_+(\vec{r},t_0)M_-(\vec{r}',t_0)e^{i\Lambda(\vec{r}',\vec{r})(t'-t_0)} \\ &-M_-(\vec{r},t_0)M_+(\vec{r}',t_0)e^{-i\Lambda(\vec{r}',\vec{r})(t'-t_0)}\Big], \end{aligned} \tag{10a}$$

$$\begin{aligned} M_\pm^{(1)}(\vec{r},t) = &\mp\frac{i\gamma\mu_0}{4\pi}e^{\left[\mp i\Delta\omega(\vec{r})-\frac{1}{T_2}\right](t-t_0)} \\ &\times\int_{t_0}^{t} dt'\int d^3\vec{r}'\; T(\vec{r}-\vec{r}')[2M_\pm(\vec{r},t_0)M_z(\vec{r}',t_0) \\ &+M_z(\vec{r},t_0)M_\pm(\vec{r}',t_0)e^{\mp i\Lambda(\vec{r}',\vec{r})(t'-t_0)}\Big], \end{aligned} \tag{10b}$$

where

$$\Lambda(\vec{r}',\vec{r}) \equiv \Delta\omega(\vec{r}') - \Delta\omega(\vec{r}) \tag{11}$$

is the susceptibility-induced frequency difference between positions $\vec{r}'$ and $\vec{r}$ of the sample.

2.2. Evolution of the magnetization after a $\pi/2$ rf pulse

As an illustration of the integral form of the Bloch equation obtained above, we examine briefly the time evolution of the magnetization when a $\pi/2$ rf pulse is applied to a system in equilibrium with the static field. Before the $\pi/2$ pulse is applied at time t_0, the magnetization is given by

$$M_\pm(\vec{r},t<t_0)=0, \quad M_z(\vec{r},t<t_0) = M_0(\vec{r}), \tag{12}$$

where $M_0(\vec{r})$ is the equilibrium magnetization. Immediately after the $\pi/2$ pulse, the magnetization becomes [37]

$$M_\pm(\vec{r},t_0) = \pm iM_0(\vec{r})e^{\pm i\phi_1}, \quad M_z(\vec{r},t_0) = 0, \tag{13}$$

where ϕ_1 is the phase of the rf pulse. This gives $M_z^{(0)}(\vec{r},t>t_0) = M_\pm^{(1)}(\vec{r},t>t_0) = 0$ according to Eqs. (9) and (10).

Eq. (7b) can be written in an alternative form by utilizing $M_z(\vec{r},t_0)=0$ and expressing the longitudinal component of the magnetization in terms of the transverse components:

$$\begin{aligned} M_\pm(\vec{r},t) = M_\pm(\vec{r},t_0)e^{\left[\mp i\Delta\omega(\vec{r})-\frac{1}{T_2}\right](t-t_0)} &\mp\frac{1}{2}\left(\frac{\gamma\mu_0}{4\pi}\right)^2\int_{t_0}^{t}dt'\int_{t_0}^{t'}dt''\int d^3\vec{r}' \\ &\times\int d^3\vec{r}''\; e^{\left[\mp i\Delta\omega(\vec{r})-\frac{1}{T_2}\right](t-t')}\{2M_\pm(\vec{r},t')T(\vec{r}-\vec{r}') \\ &\times[M_+(\vec{r}',t'')T(\vec{r}'-\vec{r}'')M_-(\vec{r}'',t'') \\ &-M_-(\vec{r}',t'')T(\vec{r}'-\vec{r}'')M_+(\vec{r}'',t'')] \\ &+T(\vec{r}-\vec{r}')M_\pm(\vec{r}',t')[M_+(\vec{r},t'')T(\vec{r}-\vec{r}'')M_-(\vec{r}'',t'') \\ &-M_-(\vec{r},t'')T(\vec{r}-\vec{r}'')M_+(\vec{r}'',t'')]\}. \end{aligned} \tag{14}$$

Recall that there is no first order DDF term in the transverse magnetization at time $t>t_0$ ($M_\pm^{(1)}(\vec{r},t>t_0)=0$). Inspection of Eq. (14) indicates that, after the $\pi/2$ pulse, the odd order DDF terms in the transverse magnetization vanish. Moreover, all the even order DDF terms have the same ϕ_1 dependence as the initial transverse magnetization. On the other hand, residual longitudinal magnetization arises after the $\pi/2$ pulse due to the DDF effect according to Eq. (7a). As can be seen in Eq. (7a), the even order DDF terms of the residual longitudinal magnetization originate from the odd order DDF terms of the transverse magnetization. By the observation for the transverse magnetization above, it is found that there is no even order DDF term in the longitudinal magnetization. Furthermore, all the odd order DDF terms of the longitudinal magnetization are independent of the phase ϕ_1. These results can be summarized as

$$\begin{cases} M_\pm^{(2m)}(\vec{r},t) \propto e^{\pm i\phi_1}, & M_z^{(2m)}(\vec{r},t) = 0, \\ M_\pm^{(2m+1)}(\vec{r},t) = 0, & M_z^{(2m+1)}(\vec{r},t) \propto e^{0i\phi_1}, \end{cases} \tag{15}$$

where m is any nonnegative integer.

In the case when the resonance frequency offset $\Delta\omega(\vec{r})$ is uniform (i.e., $\Lambda(\vec{r}',\vec{r})=0$), Eqs. (13) and (14) show that the second order DDF term of the transverse magnetization vanishes ($M_\pm^{(2)}(\vec{r},t)=0$). In addition, Eq. (14) indicates that all the higher order DDF terms of the transverse magnetization depend on the first and second order terms. As a result, all the DDF corrections to the transverse magnetization after the $\pi/2$ pulse vanish, i.e., $M_\pm(\vec{r},t) = M_\pm^{(0)}(\vec{r},t) = \pm iM_0(\vec{r})e^{\pm i\phi_1-(t-t_0)/T_2}$. This result, together with Eq. (7a), implies that there is no residual longitudinal magnetization after the $\pi/2$ pulse. It is then concluded that, when the local field distribution is uniform, the dipolar field has no effect on the evolution of the magnetization after a $\pi/2$ pulse is applied to a system in equilibrium with the static field, even though the spin density distribution is inhomogeneous. Note that the same results can also be deduced by realizing $M_z(\vec{r},t_0)=0$ and $\partial M_z(\vec{r},t)/\partial t|_{t_0=0}=0$ from Eqs. (1a) and (13). It is remarked that the results obtained above generally do not hold when T_1 relaxation is taken into account.

Finally it is observed from Eq. (15) that, when a $\pi/2$ pulse is applied to a system in equilibrium, a change of the phase ϕ_1 of the pulse has no effect on the subsequent evolution of the longitudinal magnetization. The change only affects the evolution of the transverse magnetization as a multiplicative factor $e^{i\phi_1}$ or $e^{-i\phi_1}$, which is the same for all the terms in Eq. (8). Nontrivial dependence of the magnetization upon ϕ_1 appears only after the application of at least an additional rf pulse. This will be examined using the CRAZED sequence in the next subsection.

2.3. The ϕ_1 dependence of the magnetization in the CRAZED sequence

In this subsection, the dependence of the magnetization on the phase of the first rf pulse of the CRAZED sequence (ϕ_1) is examined using the results developed above. It will be shown in the following that the knowledge of the ϕ_1 dependence of the magnetization is useful in the identification of the orders of the DDF effect in the signal when there is a susceptibility-induced field.

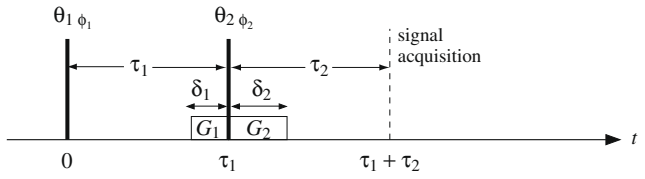

Fig. 1. The correlation spectroscopy by asymmetric z-gradient echo detection (CRAZED) sequence: it is composed of two rf pulses with flip angles (θ_1,θ_2) and phases (ϕ_1,ϕ_2), respectively applied at times $t=0$ and τ_1. The two rf pulses rotate the magnetization by the flip angles θ_1 and θ_2 about the directions $\cos\phi_1\,\hat{x}+\sin\phi_1\,\hat{y}$ and $\cos\phi_2\,\hat{x}+\sin\phi_2\,\hat{y}$, respectively. Two field gradients, $\vec{G}_1$ and $\vec{G}_2$ with durations δ_1 and δ_2, are applied right before and after the second rf pulse.

The CRAZED sequence (Fig. 1) is the most extensively used pulse sequence to form the DDF signal and is used for the studies in this paper. It is composed of two rf pulses and two field gradients, which are applied immediately before and after the second rf pulse. The durations of the rf pulses and the field gradients in the CRAZED sequence are assumed to be short enough that the effects of the dipolar field, the susceptibility-induced field, and the transverse relaxation during their applications can be ignored (hard pulse assumption). It is however remarked that these effects should be taken into account when a series of field gradients or rf pulses with finite durations is used in a pulse sequence, such as that encountered in multiple spin-echo experiments [35,38]. In the following discussions, the notations for the durations of the two field gradients (δ_1 and δ_2) are retained to indicate the timing of the pulse sequence, even though the durations are taken to be very short.

In order to maximize the dipolar field signal of the CRAZED sequence, the flip angle of the first rf pulse of the sequence is taken to be $\pi/2$. With the DDF effect during the field gradients ignored, immediately before the second rf pulse, Eq. (15) shows that

$$\begin{cases} M_{\pm}^{(2m)}(\vec{r},\tau_1^-) \propto e^{\pm i\phi_1}, & M_z^{(2m)}(\vec{r},\tau_1^-)=0, \\ M_{\pm}^{(2m+1)}(\vec{r},\tau_1^-)=0, & M_z^{(2m+1)}(\vec{r},\tau_1^-) \propto e^{0i\phi_1}. \end{cases} \tag{16}$$

The second rf pulse tips parts of $M_+(\vec{r},\tau_1^-)$ and $M_-(\vec{r},\tau_1^-)$ to the longitudinal direction and mixes the phase factors $e^{i\phi_1}$ and $e^{-i\phi_1}$ in the remaining parts of the transverse magnetization irrespective to the phase of the second rf pulse [37]. The parts of $M_+(\vec{r},\tau_1^-)$ and $M_-(\vec{r},\tau_1^-)$ that are tipped to the longitudinal direction introduce the phase factors $e^{i\phi_1}$ and $e^{-i\phi_1}$ to the longitudinal magnetization. This means that $M_\pm(\vec{r},\tau_1^-)$ give the phase dependence of $e^{i\phi_1}$ and $e^{-i\phi_1}$ to both the transverse and longitudinal components of the magnetization right after the second rf pulse. Similarly, the second rf pulse rotates part of $M_z(\vec{r},\tau_1^-)$ onto the transverse plane, and the phase factor $e^{i0\phi_1}$ of $M_z(\vec{r},\tau_1^-)$ enters into both the transverse and longitudinal components of the magnetization immediately after the second rf pulse. With the DDF effect during the second field gradient ignored, the ϕ_1 dependence of the magnetization immediately after the second field gradient that undergoes n_1 dipolar field interactions during the first evolution period is then, according to Eq. (16), given by

$$\vec{M}^{(n_1)}(\vec{r},\tau_1+\delta_2) \propto \begin{cases} e^{i\phi_1} \text{ and } e^{-i\phi_1}, & \text{for} \quad n_1=2m, \\ e^{0i\phi_1}, & \text{for} \quad n_1=2m+1. \end{cases} \tag{17}$$

During the free evolution time after the second field gradient, the transverse magnetization evolves under the influence of the distant dipolar field according to Eq. (7b). The transverse magnetization that undergoes n_2 dipolar field interactions during the second evolution period is proportional to the product of (n_2+1)'s $M_i(t_0=\tau_1+\delta_2)$, where i represents either the transverse or the longitudinal component. Taking into account the previous n_1 dipolar field interactions during the first free evolution period, the ϕ_1 dependence of the nth order dipolar field term in the transverse magnetization can be obtained by the multiplication of the phase factors of $M_i^{(n_1)}(\tau_1+\delta_2)$ by (n_2+1) times with $n_1+n_2=n$. By using Eq. (17), the ϕ_1 dependence of the nth order dipolar field term in the transverse magnetization $(M_+^{(n)}(\tau_1+\tau_2))$ at the end of the CRAZED sequence can be obtained. Examples of the result are shown in Table 1.

The ϕ_1 dependence of $M_+^{(n)}(\tau_1+\tau_2)$ keeps certain record of the order of the DDF effect, even when the magnetization is inhomogeneous in the presence of a susceptibility-induced field. In the special case when the magnetization is uniform and the sample takes an ellipsoidal shape, the dipolar field can be written in a localized form in the position space [32], and the DDF effect vanishes during the first evolution period of the CRAZED sequence when the T_1 relaxation is neglected [37]. Then the ϕ_1 dependence of the transverse magnetization at the end of the CRAZED sequence is given by the rows with $n_1=0$ in Table 1. This result is actually applicable to a general distribution of $M_0(\vec{r})$ as long as $\Delta\omega(\vec{r})$ is uniform (see Section 2.2). Knowing the ϕ_1 dependence of the transverse magnetization is useful for the design of the pulse sequence to acquire a particular order of the DDF signal.

The DDF signals with phase factors $e^{i0\phi_1}$ and $e^{\pm 2i\phi_1}$, which correspond, respectively, to the intermolecular zero-quantum coherence (iZQC) signal and the intermolecular double-quantum coherence (iDQC) signal in the quantum picture [39], have been the focus of the research on the DDF effect in the past decade. Since dipolar field effect is a small effect, the DDF signal with $e^{0i\phi_1}$ and $e^{\pm 2i\phi_1}$ comes mainly from the first order dipolar field terms (the $n=1$ terms in Table 1). As seen from Table 1, the first order DDF signal with $e^{0i\phi_1}$ originates not only from the DDF effect during the second evolution period $(n_1=0,n_2=1)$, but also from the unwanted residual magnetization that arises during the first evolution period $(n_1=1,n_2=0)$. On the other hand, since the first order DDF signal with $e^{\pm 2i\phi_1}$ originates entirely from the DDF effect during the second evolution period, we will focus on this part of the signal in this paper. In experiments, the DDF signal with the phase factors $e^{\pm 2i\phi_1}$ can be selected by using an area ratio 1:2 for the pair of the gradient fields, and repeating the pulse sequence with a 4-step phase cycle, where $\phi_1=(0^\circ,180^\circ,90^\circ,270^\circ)$ and the receiver phase $\phi_{\text{rec}}=(0^\circ,0^\circ,180^\circ,180^\circ)$ [40].

Table 1
The ϕ_1 dependence of the nth order dipolar field term in the transverse magnetization at the end of the CRAZED sequence, with $n=0,1,2$ and 3. The nth order DDF term of the transverse magnetization $M_+^{(n)}(\tau_1+\tau_2)$ is proportional to the product of (n_2+1)'s $M_i^{(n_1)}(\tau_1+\delta_2)$, where (n_1,n_2) are the orders of the dipolar field interaction, respectively, during the first and second evolution periods of the CRAZED sequence that give the sum $n=n_1+n_2$, and M_i represents either the transverse or the longitudinal magnetization. As described in Eq. (17), $M_\pm^{(n_1)}(\tau_1+\delta_2)$ and $M_z^{(n_1)}(\tau_1+\delta_2)$ are proportional to the phase factors $e^{i\phi_1}$ and $e^{-i\phi_1}$ for even n_1, and proportional to $e^{0i\phi_1}$ for odd n_1. The ϕ_1 dependence of $M_+^{(n)}(\tau_1+\tau_2)$ is obtained by the multiplication of the phase factors, $(e^{i\phi_1},e^{-i\phi_1})$ or $(e^{i0\phi_1})$, of $M_i^{(n_1)}(\tau_1+\delta_2)$ by (n_2+1) times.

n (n_1,n_2)	ϕ_1 in $M_i^{(n_1)}(\tau_1+\delta_2)$	Multiplication power (n_2+1)	ϕ_1 in $M_+^{(n)}(\tau_1+\tau_2)$
0 (0,0)	$(e^{i\phi_1},e^{-i\phi_1})$	1	$e^{\pm i\phi_1}$
1 (0,1)	$(e^{i\phi_1},e^{-i\phi_1})$	2	$e^{i0\phi_1}$, $e^{\pm 2i\phi_1}$
1 (1,0)	$(e^{i0\phi_1})$	1	$e^{i0\phi_1}$
2 (0,2)	$(e^{i\phi_1},e^{-i\phi_1})$	3	$e^{\pm i\phi_1}$, $e^{\pm 3i\phi_1}$
2 (1,1)	$(e^{i0\phi_1})$	2	$e^{i0\phi_1}$
2 (2,0)	$(e^{i\phi_1},e^{-i\phi_1})$	1	$e^{\pm i\phi_1}$
3 (0,3)	$(e^{i\phi_1},e^{-i\phi_1})$	4	$e^{i0\phi_1}$, $e^{\pm 2i\phi_1}$, $e^{\pm 4i\phi_1}$
3 (1,2)	$(e^{i0\phi_1})$	3	$e^{i0\phi_1}$
3 (2,1)	$(e^{i\phi_1},e^{-i\phi_1})$	2	$e^{i0\phi_1}$, $e^{\pm 2i\phi_1}$
3 (3,0)	$(e^{i0\phi_1})$	1	$e^{i0\phi_1}$

3. Magnetization evolution in the CRAZED sequence

In this section, the evolution of the magnetization in the CRAZED sequence (Fig. 1) is calculated analytically under the first order dipolar field approximation using Eqs. (8)–(10). An estimation of the error in truncating the high order terms is given in Appendix A.

The CRAZED sequence can be viewed as two parts. In the first part, an rf pulse with flip angle θ_1 is applied to the equilibrium magnetization to prepare spin coherence. The magnetization is then evolved under the DDF for a period of $\tau_1 - \delta_1$. Subsequently a field gradient of strength G_1 is applied for a duration of δ_1. In this paper, the durations of the two field gradients are taken to be very short (see Section 2.3). The flip angle of the first rf pulse is taken as $\theta_1 = \pi/2$ to maximize the dipolar field signal.

After the first rf pulse, the magnetization is given by Eq. (13). Then at the end of the first evolution period, the magnetization becomes

$$M_{\pm}(\vec{r},\tau_1^-) = \pm i M_0(\vec{r}) e^{-\frac{\tau_1}{T_2}} e^{\pm i\alpha(\vec{r})}, \tag{18a}$$

$$M_z(\vec{r},\tau_1^-) = -\frac{i}{8\pi}\gamma\mu_0 M_0(\vec{r}) \int_0^{\tau_1} dt' e^{-\frac{2t'}{T_2}} \int d^3\vec{r}'\, T(\vec{r}-\vec{r}') \times M_0(\vec{r}')\left[e^{i\Lambda(\vec{r}',\vec{r})t'} - e^{-i\Lambda(\vec{r}',\vec{r})t'}\right]. \tag{18b}$$

Here $\alpha(\vec{r}) = \phi_1 - \Delta\omega(\vec{r})\tau_1 - \gamma\vec{G}_1\cdot\vec{r}\delta_1$ is the phase acquired in the first evolution period (τ_1). The equilibrium magnetization $M_0(\vec{r}) \approx n_H(\vec{r})\hbar^2\gamma^2 B_0/(4k_B T_B)$, where $\hbar$ is the angular Planck constant, k_B is the Boltzmann factor, T_B is the temperature, B_0 is the static field strength, and $n_H(\vec{r})$ is the spin number density.

Eq. (18b) describes the residual longitudinal magnetization that arises during the first evolution period due to the dipolar field effect. It should be noted that when the local field distribution is uniform (i.e., $\Lambda(\vec{r}',\vec{r}) = 0$), the residual longitudinal magnetization during the first evolution period vanishes even when the spin density distribution is inhomogeneous. Indeed Section 2.2 shows that the dipolar field has no effect on the evolution of the magnetization after the $\pi/2$ pulse. This justifies the practice of ignoring the DDF effect for the magnetization during the first evolution period of the CRAZED sequence [18].

The second part of the CRAZED sequence starts by the second rf pulse with flip angle θ_2 and follows by the second field gradient with strength G_2 and duration δ_2. After the second field gradient, the magnetization evolves freely under the DDF for a duration of $\tau_2 - \delta_2$ before the measurement is made. Without loss of generality, the phase of the second pulse is taken as $\phi_2 = 0$. Then at $t = \tau_1^+$,

$$M_{\pm}(\vec{r},\tau_1^+) = \pm iM_0(\vec{r})e^{-\frac{\tau_1}{T_2}}\left[\cos^2\frac{\theta_2}{2}e^{\pm i\alpha(\vec{r})} - \sin^2\frac{\theta_2}{2}e^{\mp i\alpha(\vec{r})}\right] \pm i\sin\theta_2 M_z(\vec{r},\tau_1^-), \tag{19a}$$

$$M_z(\vec{r},\tau_1^+) = -\sin\theta_2 M_0(\vec{r})e^{-\frac{\tau_1}{T_2}}\cos\alpha(\vec{r}) + \cos\theta_2 M_z(\vec{r},\tau_1^-). \tag{19b}$$

By substituting Eq. (18b) into (19) and using Eqs. (8), (9) and (10), the transverse magnetization at the end of the CRAZED sequence reads as

$$M_+(\vec{r},\tau_1+\tau_2) = M_+^{(0)}(\vec{r},\tau_1+\tau_2) + M_{+,\mathrm{res}}^{(1)}(\vec{r},\tau_1+\tau_2) + M_{+,\mathrm{DDF}}^{(1)}(\vec{r},\tau_1+\tau_2), \tag{20}$$

where

$$M_+^{(0)}(\vec{r},\tau_1+\tau_2) = iM_0(\vec{r})e^{-\frac{\tau_1+\tau_2}{T_2}}e^{i\beta(\vec{r})}\left\{\cos^2\frac{\theta_2}{2}e^{i\alpha(\vec{r})} - \sin^2\frac{\theta_2}{2}e^{-i\alpha(\vec{r})}\right\}, \tag{21}$$

$$M_{+,\mathrm{res}}^{(1)}(\vec{r},\tau_1+\tau_2) = \frac{A_{\theta_2}M_0(\vec{r})}{2(2\pi)^3}e^{-\frac{\tau_2}{T_2}}e^{i\beta(\vec{r})}\int_0^{\tau_1}dt'e^{-\frac{2t'}{T_2}}\int d^3\vec{r}'\,T(\vec{r}-\vec{r}')M_0(\vec{r}') \times\left[e^{i\Lambda(\vec{r}',\vec{r})t'} - e^{-i\Lambda(\vec{r}',\vec{r})t'}\right], \tag{22a}$$

and

$$\begin{aligned} M_{+,\mathrm{DDF}}^{(1)}(\vec{r},\tau_1+\tau_2) &= -\frac{2A_{\theta_2}M_0(\vec{r})}{(2\pi)^3}\tau_2 e^{-\frac{2\tau_1+\tau_2}{T_2}}\left\{\cos^2\frac{\theta_2}{2}e^{i\alpha(\vec{r})} - \sin^2\frac{\theta_2}{2}e^{-i\alpha(\vec{r})}\right\}e^{i\beta(\vec{r})} \\ &\times\int d^3\vec{r}'\,T(\vec{r}-\vec{r}')M_0(\vec{r}')\cos\alpha(\vec{r}') \\ &-\frac{A_{\theta_2}M_0(\vec{r})}{(2\pi)^3}\cos\alpha(\vec{r})e^{-\frac{2\tau_1+\tau_2}{T_2}}e^{-i\Delta\omega(\vec{r})\tau_2}\int_{\tau_1}^{\tau_1+\tau_2}dt' \\ &\times\int d^3\vec{r}'\,T(\vec{r}-\vec{r}')M_0(\vec{r}')e^{-i\Lambda(\vec{r}',\vec{r})(t'-\tau_1)} \\ &\times e^{-i\gamma\vec{G}_2\cdot\vec{r}'\delta_2}\left\{\cos^2\frac{\theta_2}{2}e^{i\alpha(\vec{r}')} - \sin^2\frac{\theta_2}{2}e^{-i\alpha(\vec{r}')}\right\}. \end{aligned} \tag{22b}$$

Here $A_{\theta_2} = \frac{1}{4\pi}(2\pi)^3\sin\theta_2\gamma\mu_0$ and $\beta(\vec{r}) = -\Delta\omega(\vec{r})\tau_2 - \gamma\vec{G}_2\cdot\vec{r}\delta_2$ is the phase acquired in the second evolution period (τ_2).

The term $M_+^{(0)}$ is the zeroth order dipolar field approximation of the transverse magnetization. It depends on the phase factors $e^{i\phi_1}$ and $e^{-i\phi_1}$. The term $M_{+,\mathrm{res}}^{(1)}$ comes from the residual longitudinal magnetization arising during the first evolution period due to the DDF, which is flipped to the transverse plane by the second rf pulse. Note that this term is independent of ϕ_1. The magnitude of $M_{+,\mathrm{res}}^{(1)}$ is much smaller than that of $M_{+,\mathrm{DDF}}^{(1)}$ when $\tau_1 \ll \tau_2$, and is zero when $\Delta\omega(\vec{r})$ is uniform. The term $M_{+,\mathrm{DDF}}^{(1)}$ describes the first order dipolar field approximation of the transverse magnetization that is evolved under the influence of the dipolar field after the second rf pulse of the pulse sequence. It depends on the phase factors $e^{0i\phi_1}$, $e^{2i\phi_1}$ and $e^{-2i\phi_1}$. We will focus on those terms with the phase factors $e^{\pm 2i\phi_1}$ (see Section 2.3).

Eq. (22) can be recast in a simpler form for numerical calculations in k-space. First, we introduce the susceptibility-modulated magnetization

$$\mathscr{M}(\vec{r},t) \equiv M_0(\vec{r})e^{i\Delta\omega(\vec{r})t}, \tag{23}$$

of which the Fourier transform is defined by

$$\widetilde{\mathscr{M}}(\vec{k},t) = \frac{1}{(2\pi)^3}\int d^3\vec{r}\,\mathscr{M}(\vec{r},t)\,e^{-i\vec{k}\cdot\vec{r}}. \tag{24}$$

For any wave vector $\vec{g}$, we have

$$\int d^3\vec{r}'\,T(\vec{r}-\vec{r}')\mathscr{M}(\vec{r}',t)e^{i\vec{g}\cdot\vec{r}'} = (2\pi)^3\int d^3\vec{k}\;\widetilde{T}(\vec{k})\,\widetilde{\mathscr{M}}(\vec{k}-\vec{g},t)\,e^{i\vec{k}\cdot\vec{r}}. \tag{25}$$

By substituting Eq. (25) into Eq. (22), the first order dipolar field approximation of the transverse magnetization at the end of the CRAZED sequence can be rewritten in the k-space representation as

$$M_{+,\mathrm{res}}^{(1)}(\vec{r},\tau_1+\tau_2) = \frac{1}{2}A_{\theta_2}M_0(\vec{r})e^{-\frac{\tau_2}{T_2}}e^{i\beta(\vec{r})}\int d^3\vec{k}\;\widetilde{T}(\vec{k})e^{i\vec{k}\cdot\vec{r}}\int_0^{\tau_1}dt'\,e^{-\frac{2t'}{T_2}} \times\left\{e^{-i\Delta\omega(\vec{r})t'}\,\widetilde{\mathscr{M}}(\vec{k},t') - e^{i\Delta\omega(\vec{r})t'}\,\widetilde{\mathscr{M}}(\vec{k},-t')\right\}, \tag{26a}$$

$$\begin{aligned} M_{+,\mathrm{DDF}}^{(1)}(\vec{r},\tau_1+\tau_2) &= -A_{\theta_2}M_0(\vec{r})\tau_2 e^{-\frac{2\tau_1+\tau_2}{T_2}}e^{i\beta(\vec{r})}\left[\cos^2\frac{\theta_2}{2}e^{i\alpha(\vec{r})} - \sin^2\frac{\theta_2}{2}e^{-i\alpha(\vec{r})}\right] \\ &\times\int d^3\vec{k}\;\widetilde{T}(\vec{k})e^{i\vec{k}\cdot\vec{r}}\left\{e^{i\phi_1}\,\widetilde{\mathscr{M}}(\vec{k}+\vec{g}_1,-\tau_1) + e^{-i\phi_1}\,\widetilde{\mathscr{M}}(\vec{k}-\vec{g}_1,\tau_1)\right\} \\ &-A_{\theta_2}M_0(\vec{r})\cos\alpha(\vec{r})e^{-\frac{2\tau_1+\tau_2}{T_2}}e^{-i\Delta\omega(\vec{r})(\tau_2+\tau_1)}\int d^3\vec{k}\;\widetilde{T}(\vec{k})e^{i\vec{k}\cdot\vec{r}} \\ &\times\int_{\tau_1}^{\tau_1+\tau_2}dt'\,e^{i\Delta\omega(\vec{r})t'}\left\{\cos^2\frac{\theta_2}{2}e^{i\phi_1}\,\widetilde{\mathscr{M}}(\vec{k}+\vec{g}_2+\vec{g}_1,-t')\right. \\ &\left.-\sin^2\frac{\theta_2}{2}e^{-i\phi_1}\,\widetilde{\mathscr{M}}(\vec{k}+\vec{g}_2-\vec{g}_1,-t'+2\tau_1)\right\}, \end{aligned} \tag{26b}$$

where

$$\vec{g}_1 = \gamma \vec{G}_1 \delta_1 \quad \text{and} \quad \vec{g}_2 = \gamma \vec{G}_2 \delta_2 \tag{27}$$

denote the modulation wave vectors induced by the gradient fields.

For liquid, the measured MR signal of a particular region comes from the sum of the transverse magnetization over the volume of that region. After summing over the sample volume, the form of the DDF signal obtained in Eq. (26b) is similar to that obtained in Ref. [14]. The main difference is that, in additional to the Fourier space integral of the equilibrium magnetization distribution, the second term of Eq. (26b) also involves a temporal integral of the susceptibility-induced frequency distribution. This suggests that Eq. (26b) may be used to obtain the Patterson function to assess the length scales of the local field variations.

Eq. (26) can be used to calculate the DDF signal when the distributions of the equilibrium magnetization and the susceptibility-induced field are given. As an illustration, we calculate the DDF signal of a sample formed in the CRAZED sequence when there is no susceptibility-induced field ($\Delta\omega(\vec{r}) = 0$). In this case, $\widetilde{\mathscr{M}}(\vec{k}, t) = \widetilde{M}_0(\vec{k})$, where $\widetilde{M}_0(\vec{k})$ is the Fourier transform of the equilibrium magnetization. By summing Eq. (26) over the volume of the sample S, the DDF signal is given by

$$\begin{aligned}\langle M_+^{(1)}(\tau_1+\tau_2)\rangle_S &= \int_S d^3\vec{r}\, M_+^{(1)}(\vec{r}, \tau_1+\tau_2)\\ &= -\frac{3}{2}(2\pi)^3 A_{\theta_2}\tau_2 e^{-\frac{2\tau_1+\tau_2}{T_2}} \int d^3\vec{k}\, \widetilde{T}(\vec{k})\\ &\times \left[\cos^2\frac{\theta_2}{2} e^{2i\phi_1}\widetilde{M}_0(\vec{k}+\vec{g}_1)\widetilde{M}_0(-\vec{k}+\vec{g}_2+\vec{g}_1)\right.\\ &- \sin^2\frac{\theta_2}{2}\widetilde{M}_0(\vec{k}+\vec{g}_1)\widetilde{M}_0(-\vec{k}+\vec{g}_2-\vec{g}_1)\\ &+ \cos^2\frac{\theta_2}{2}\widetilde{M}_0(\vec{k}-\vec{g}_1)\widetilde{M}_0(-\vec{k}+\vec{g}_2+\vec{g}_1)\\ &\left.- \sin^2\frac{\theta_2}{2} e^{-2i\phi_1}\widetilde{M}_0(\vec{k}-\vec{g}_1)\widetilde{M}_0(-\vec{k}+\vec{g}_2-\vec{g}_1)\right].\end{aligned} \tag{28}$$

Eq. (28) is equivalent to the result given in Eq. (10) of Ref. [18].

4. Sensitivity of DDF signal to sub-voxel susceptibility-induced field variations

The results of Section 3 are applied in this section to study the properties of the dipolar field signal with respect to sub-voxel susceptibility-induced field variations. The DDF signal is calculated by summing Eq. (26) over the volume of a voxel. The spatial distributions of the equilibrium magnetization $M_0(\vec{r})$ and the frequency shift $\Delta\omega(\vec{r})$ are modeled using the parameters for brain tissues, with the perturbed field arising from blood vessels.

A common way to model the susceptibility-induced field of a blood vessel is to use an infinitely long cylinder with a finite susceptibility difference from the background [21,41,42]. However, the field variation modeled by cylinders is too complicated for analysis, especially it is uncertain whether the sensitivity of the DDF signal to the sub-voxel field variations on the length scale selected by the gradient field can be observed. Therefore, we first consider a simpler model of field variation using blocks of uniform perturbed field (the block model) to shed light on the understanding of the dependence of the DDF signal on the correlation length. The results are then compared with that of the blood vessel model.

4.1. The uniform block model for susceptibility-induced field distribution

The details of the block model can be found in the Appendix B. In the block model, the sub-voxel magnetic field variation is taken to be made up of blocks of uniform frequency shifts. The equilibrium magnetization, on the other hand, is taken to be independent of position $\vec{r}$ so that the effect of the field variation on the signal formation is separated from that of the spin density distribution. To maximize the DDF signal of a voxel with finite size under the periodic condition (see the Appendix B), the modulation wave vectors of the gradient fields are taken to be integral multiples of the inverse of the voxel period, i.e., $\vec{g}_i = \{\frac{2\pi}{l_x}m, \frac{2\pi}{l_y}p, \frac{2\pi}{l_z}q\}$, where $\{l_x, l_y, l_z\}$ are the dimensions of the voxel, $\{m, p, q\}$ are integers, and $i = 1, 2$ denote the indices of the first and second gradient fields.

In the calculations, we consider N_b identical tubes of uniform frequency shifts lying along the x-direction. Each tube is taken to have dimensions $l_x \times a_y \times a_z$, volume $\Delta v = l_x a_y a_z$, and frequency shift c. The position of the center of the ith tube is located at $\vec{r}_{0i} = \{0, y_{0i}, z_{0i}\}$ inside the voxel with volume $v = l_x l_y l_z$, where $i = 1, \cdots, N_b$. The modulations of the two field gradients are taken to be along the z-direction ($\widehat{G}_2 = \widehat{G}_1 = \hat{z}$) and the area ratio is taken as $G_2\delta_2 = 2G_1\delta_1$. Then the DDF signal of the voxel (the total transverse magnetization over the voxel volume v) with phase factors $e^{\pm 2i\phi_1}$ normalized by that of the case with uniform field distribution can be expressed in terms of different explicit orders of the volume ratio of the tubes ($\Delta v/v$) as

$$\frac{\langle M_{+,2\phi_1}^{(1)}\rangle_v}{\langle M_{+,2\phi_1}^{(1)}\rangle_{v,\Delta v=0}} = 1 + \frac{\langle M_+^{(1,b)}\rangle_v}{\langle M_{+,2\phi_1}^{(1)}\rangle_{v,\Delta v=0}} + \frac{\langle M_+^{(1,c)}\rangle_v}{\langle M_{+,2\phi_1}^{(1)}\rangle_{v,\Delta v=0}}, \tag{29}$$

with

$$\frac{\langle M_+^{(1,b)}\rangle_v}{\langle M_{+,2\phi_1}^{(1)}\rangle_{v,\Delta v=0}} = \frac{\Delta v}{v}\sum_{i=1}^{N_b}\left[h_1(-\tau_1,\tau_2) - \eta e^{-4ig_1 z_{0i}}\operatorname{sinc}(2g_1 a_z) h_1(\tau_1,\tau_2)\right], \tag{30a}$$

$$\begin{aligned}\frac{\langle M_+^{(1,c)}\rangle_v}{\langle M_{+,2\phi_1}^{(1)}\rangle_{v,\Delta v=0}} &= \frac{\Delta v^2}{v^2}\sum_{i=1}^{N_b}\sum_{j=1}^{N_b}\sum_{p,q=-\infty}^{\infty}\frac{\widetilde{T}(\vec{k}_{0pq}+\vec{g}_1)}{\widetilde{T}(\vec{g}_1)}\left\{h_2(-\tau_1,\tau_2)\right.\\ &\times e^{i\vec{k}_{0pq}\cdot(\vec{r}_{0j}-\vec{r}_{0i})}\operatorname{sinc}^2\left(\frac{p\pi a_y}{l_y}\right)\operatorname{sinc}^2\left(\frac{q\pi a_z}{l_z}\right)\\ &- \eta h_2(\tau_1,\tau_2) e^{i(\vec{k}_{0pq}-2\vec{g}_1)\cdot\vec{r}_{0j}} e^{-i(\vec{k}_{0pq}+2\vec{g}_1)\cdot\vec{r}_{0i}}\operatorname{sinc}^2\left(\frac{p\pi a_y}{l_y}\right)\\ &\left.\times\operatorname{sinc}\left(\frac{q\pi a_z}{l_z}+g_1 a_z\right)\operatorname{sinc}\left(\frac{q\pi a_z}{l_z}-g_1 a_z\right)\right\},\end{aligned} \tag{30b}$$

where $\eta = e^{4i\phi_1}\cot^2\frac{\theta_2}{2}$, $g_1 = \gamma G_1\delta_1$, the wave vector $\vec{k}_{mpq} = \{\frac{2\pi}{l_x}m, \frac{2\pi}{l_y}p, \frac{2\pi}{l_z}q\}$ takes only discrete values due to the periodic condition imposed on the voxel, and

$$h_1(\tau_1,\tau_2) = \frac{2}{3}e^{-\frac{i}{2}c(\tau_2+2\tau_1)}\left[2\cos\frac{c\tau_2}{2} + \operatorname{sinc}\frac{c\tau_2}{2}\right] - 2, \tag{31a}$$

$$h_2(\tau_1,\tau_2) = -h_1(\tau_1,\tau_2) + \left[e^{-ic(\tau_2+2\tau_1)} - 1\right]. \tag{31b}$$

It should be noted that the function h_1 in $\langle M_+^{(1,b)}\rangle_v$ oscillates in τ_1 and τ_2 at the single frequency c, while the function h_2 in $\langle M_+^{(1,c)}\rangle_v$ oscillates in τ_2 at the single frequency c and oscillates in τ_1 at both the single frequency c and the compound frequency $2c$.

Eq. (30) shows that, with the field variation modeled by blocks of uniform frequency shifts, the phase induced by the gradient fields vanishes when there is only one tube located at the center of the voxel ($\vec{r}_{01} = \vec{0}$). In this case, the dephasing effect of the perturbed field can be treated separately from that of the gradient

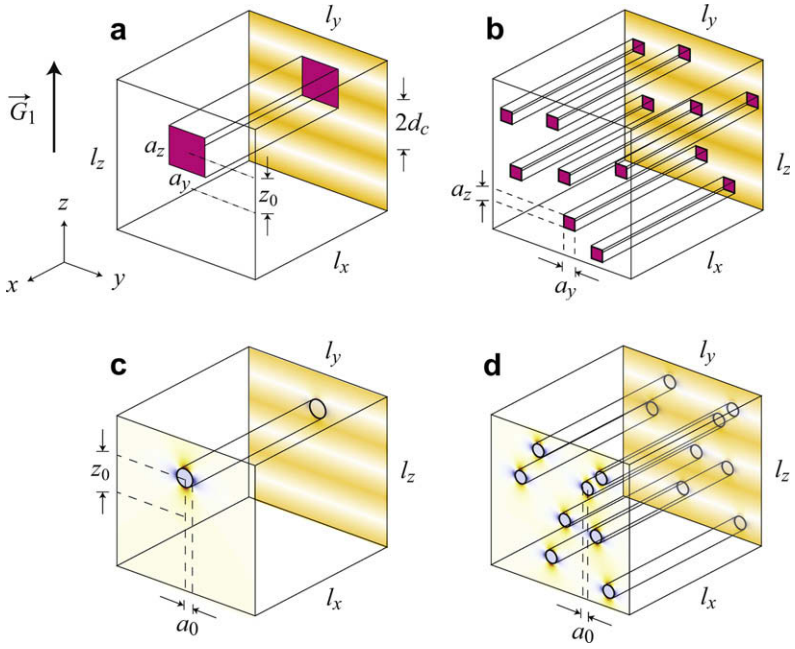

Fig. 2. Schematic of the voxel with the susceptibility-induced frequency distribution modeled by (a) a single square tube of frequency shift c and volume $\Delta v = l_x a_y a_z$ placed at a distance z_0 from the center of the voxel, (b) N_b square tubes with the same frequency shift and dimension placed randomly in the voxel, (c) a cylinder with volume $\Delta v = \pi l_x a_0^2$ and a susceptibility difference $\Delta\chi_0$ from the background placed at a displacement of z_0 from the center of the voxel, and (d) N_c cylinders with the same dimension and susceptibility difference from the background placed randomly in the voxel. The tubes and the cylinders are placed along the x-direction. Inside the voxel, the equilibrium magnetization distribution M_0 is taken to be uniform. The field gradient is taken to modulate the magnetization along the z-direction. The modulation depicted on the back surface of the voxel illustrates the spatial dependent phase in the magnetization imposed by the field gradient $\vec{G}_1$. The correlation length d_c is defined in Eq. (32).

field. The two dephasing effects will be analyzed in detail in the following numerical calculations.

4.2. Parameters for the numerical calculations

Numerical calculations are carried out using Eqs. (29), (30) and (31) derived for the block model with the perturbed field modeled by square tubes of uniform resonance frequency shifts. The susceptibility-induced frequency distributions used in these calculations are depicted in Fig. 2a and b. Such field distributions are analogous to the susceptibility-induced field of infinitely long cylinders placed parallel to the static field, which is constant inside the cylinders and zero elsewhere [41]. Corresponding calculations are then performed using Eq. (26) with the perturbed field modeled by infinitely long cylinders with a finite susceptibility difference from the background (the blood vessel model). The susceptibility-induced frequency distributions used in the blood vessel model calculations are depicted in Fig. 2c and d.

In the calculations, the area ratio of the field gradients is taken as $G_2\delta_2 = 2G_1\delta_1$ and the modulation is taken to be along the z-direction. The correlation length is defined as

$$d_c \equiv \frac{\pi}{\gamma G_1 \delta_1} = \frac{\pi}{g_1}. \tag{32}$$

The second rf pulse is set at the optimal flip angle $\theta_2 = 2\pi/3$ [43]. Parameters of brain at $B_0 = 9.4$ T and temperature $T_B = 300$ K are used: transverse relaxation time $T_2 = 40$ ms and proton number density $n_H = 0.78 n_{\text{water}}$ [33,44], where n_{water} is the proton number density of pure water. The frequency shift c of the tubes in the block model is chosen to be 0.045–0.36 ppm (in units of γB_0) to simulate the approximate amplitude of the local field induced by deoxygenated blood in the brain, whereas the susceptibility of the cylinders of the blood vessel model is taken as 2.16 ppm to compare the results with the block model. The total volume ratios of the tubes and the cylinders are chosen to be 0–9.6%.

The DDF signals with phase factors $e^{\pm 2i\phi_1}$ as calculated for the block model and the blood vessel model will be denoted by $\langle M_+ \rangle_v$ in the following for simplicity.

4.3. Calculations with the block model

The dipolar field signal is dephased by both the susceptibility-induced field and the gradient field. For the field variation described by blocks of uniform frequency shift, the phase induced by the gradient fields vanishes when $\vec{r}_{0i} = \vec{0}$ (see Eq. (30)). To study the DDF signal dependence on the phase induced by the perturbed field, the dephasing effect of the gradient fields is suppressed for the moment by considering a single tube of frequency shift c placed at the center of the voxel (Fig. 2a with $z_0 = 0$).

As can be seen from Eq. (29), the difference of the DDF signal in the presence of the perturbed field from that of the case with uniform field distribution increases with the volume ratio $\Delta v/v$. The difference of the normalized signal from that with uniform field distribution is given by

$$\Delta m_+(\tau_1, \tau_2) \equiv 1 - \left| \frac{\langle M_+(\tau_1, \tau_2) \rangle_v}{\langle M_+(\tau_1, \tau_2) \rangle_{v, \Delta v = 0}} \right|. \tag{33}$$

The DDF signal, and hence $\Delta m_+(\tau_2)$, oscillates in τ_1 and τ_2 through the h functions given in Eq. (31). When the volume ratio of the perturbed field region is much smaller than unity ($\Delta v/v \ll 1$), the amplitude and the oscillation frequencies of Δm_+ are mainly contributed by Eq. (30a) because Eq. (30b) is quadratic in $\Delta v/v$. The average of Eq. (33) over τ_2 as denoted by $\overline{\Delta m_+}$ is plotted versus the tube volume ratio in Fig. 3. As shown in the figure, $\overline{\Delta m_+}$ increases with $\Delta v/v$, and is nearly linear in $\Delta v/v$ when $\Delta v/v \ll 1$. On the other hand, it is observed in the inset of Fig. 3b that the amplitude of $\overline{\Delta m_+}$ oscillates with the frequency shift (c), and is about to complete one cycle when c is changed by 0.225 ppm. According to Eq. (30a), $\langle M_+^{(1,b)} \rangle$, and hence Δm_+, depends on the

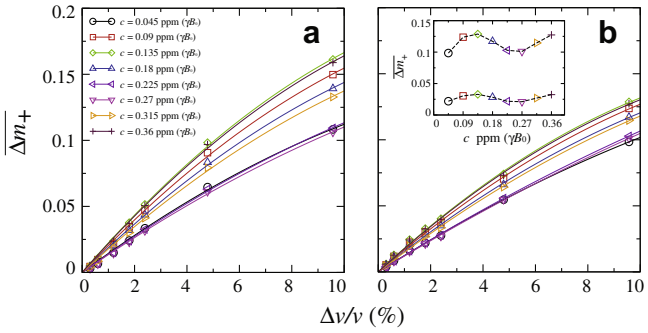

Fig. 3. Plot of the average normalized signal difference $\overline{\Delta m_+}$ as a function of the volume ratio $\Delta v/v$ with (a) $\gamma G_1\delta_1 = 2(2\pi/l_z)$ and (b) $\gamma G_1\delta_1 = 4(2\pi/l_z)$ for various frequency shifts c. The data points are the numerical calculated values and the solid lines are the quadratic fits of the data. The inset in (b) shows the plot of $\overline{\Delta m_+}$ as a function of c for $\gamma G_1\delta_1 = 4(2\pi/l_z)$ and $\Delta v/v = 1.8\%$ and 9.6%. Parameters used are: $\phi_1 = 0$, $\tau_1 = 10$ ms and number of grid points = $128 \times 128 \times 256$.

phase factors $e^{ic\tau_1}$ and $e^{ic\tau_2}$ through h_1. Thus for a fixed τ_1, the average of Δm_+ over τ_2 ($\overline{\Delta m_+}$) oscillates with c. When c is changed by $2\pi/(\gamma B_0\tau_1) \sim 0.25$ ppm, the oscillation of $\overline{\Delta m_+}$ completes a cycle, and $\overline{\Delta m_+}$ returns to the same amplitude as can be seen in Fig. 3.

The acquisition time for maximal DDF signal is $\tau_2 \sim T_2$ [3], which is different from the refocusing time $2\tau_1$ [45] with the considered parameters. To study the signal dependence on the correlation length, the normalized total transverse magnetizations ($|\langle M_+\rangle_v|/|\langle M_+\rangle_{v,\Delta v=0}|$) at $\tau_2 = T_2$ and $2\tau_1$ are plotted against the modulation wave vector ($g_1 = \gamma G_1\delta_1$) in Fig. 4. It can be seen in the figure that the amplitude of $|\langle M_+\rangle_v|/|\langle M_+\rangle_{v,\Delta v=0}|$ varies for different c. This signal variation originates from the phase induced by the perturbed field during the free evolution periods. Such phase dependence is manifested in the h functions as we have discussed previously for Fig. 3. When the DDF signal is calculated at $\tau_2 = 2\tau_1$ as in Fig. 4d–f, the dependence on the phase induced by the perturbed field during the evolution periods, and hence the variation of the signal, is minimized.

It is noted in Fig. 4 that the amplitude of $|\langle M_+\rangle_v|/|\langle M_+\rangle_{v,\Delta v=0}|$ for $\tau_2 = 2\tau_1$ approaches unity for large tube size ($\Delta v/v$) and large gradient field strength ($\gamma G_1\delta_1$). These limits correspond to the regime where the correlation length ($d_c = \pi/g_1$) is much smaller than the characteristic length of the field variation (a_z). It is seen from Eq. (31) that $h_2(-\tau_1, 2\tau_1) = -h_1(-\tau_1, 2\tau_1)$, and from Eq. (30),

$$\mathrm{sinc}(2g_1a_z) \approx 0,$$

$$\sum_{p,q=-\infty}^{\infty} \frac{\widetilde{T}(\vec{k}_{0pq}+\vec{g}_1)}{\widetilde{T}(\vec{g}_1)} \mathrm{sinc}^2\left(\frac{p\pi a_y}{l_y}\right) \mathrm{sinc}\left(\frac{q\pi a_z}{l_z}+g_1a_z\right) \mathrm{sinc}\left(\frac{q\pi a_z}{l_z}-g_1a_z\right) \approx 0,$$

$$\sum_{p,q=-\infty}^{\infty} \frac{\widetilde{T}(\vec{k}_{0pq}+\vec{g}_1)}{\widetilde{T}(\vec{g}_1)} \mathrm{sinc}^2\left(\frac{p\pi a_y}{l_y}\right) \mathrm{sinc}^2\left(\frac{q\pi a_z}{l_z}\right) \approx v/\Delta v,$$

when $g_1l_z > g_1a_z \gg \pi$. Then the second and third terms of Eq. (29) cancel each other, giving $|\langle M_+\rangle_v|/|\langle M_+\rangle_{v,\Delta v=0}| \to 1$. In these limits, the effect of the field variation on the DDF signal formation becomes

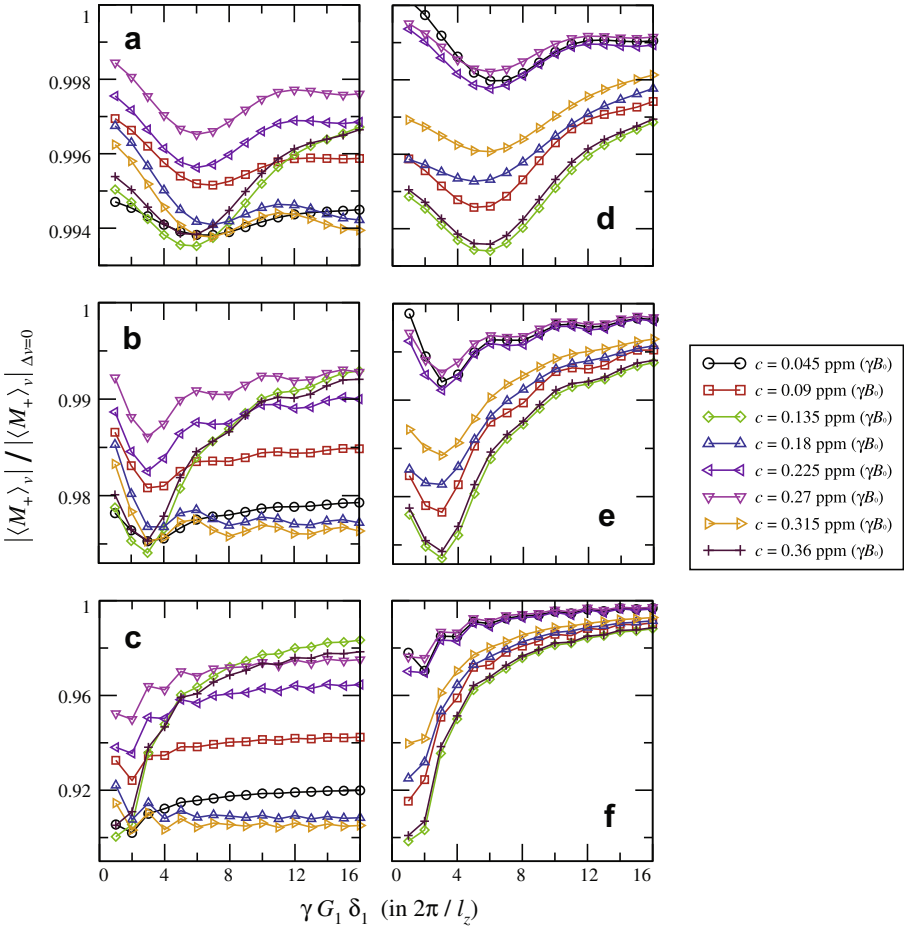

Fig. 4. Plot of the normalized total transverse magnetization as a function of $\gamma G_1\delta_1$ at time $\tau_2 = T_2$ (a–c) and $\tau_2 = 2\tau_1$ (d–f) for various frequency shifts (c) and volume ratios: (a and d) $\Delta v/v = 0.3\%$, (b and e) $\Delta v/v = 1.2\%$, and (c and f) $\Delta v/v = 4.8\%$. Parameters used are: $\phi_1 = 0$, $\tau_1 = 10$ ms and number of grid points = $128 \times 128 \times 256$.

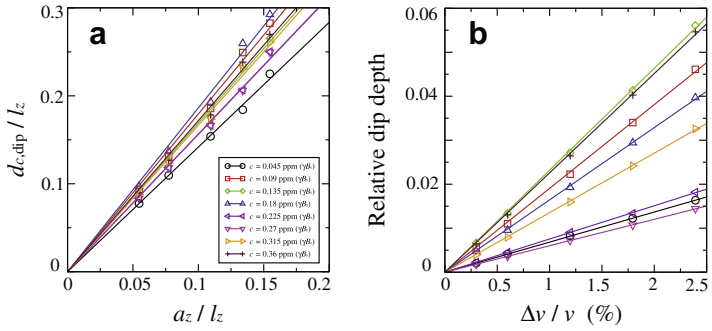

Fig. 5. Plots of (a) the correlation distance that corresponds to the dip position of the DDF signal against the width of the tube and (b) the corresponding dip depth against the volume ratio of the tube for $\tau_2 = 2\tau_1$ and various frequency shifts (c). The solid lines are linear fits to the numerical data.

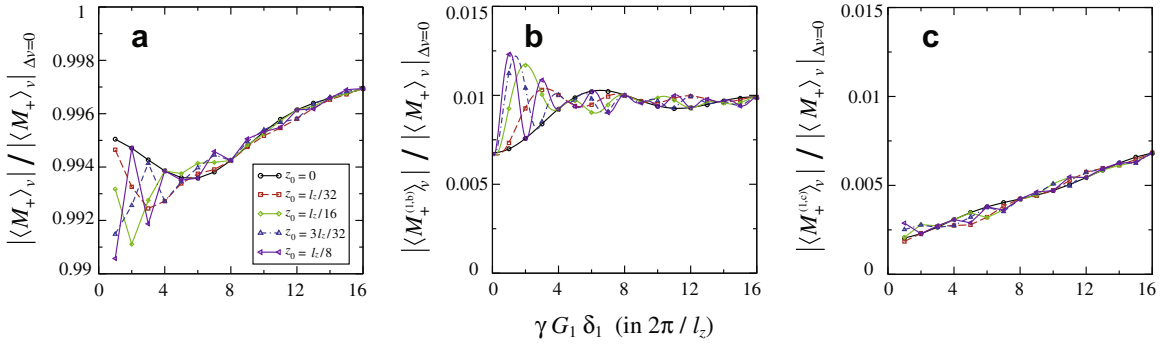

Fig. 6. Plots of (a) $|\langle M_+\rangle_v|/|\langle M_+\rangle_{v,\Delta v=0}|$, (b) $|\langle M_+^{(1,b)}\rangle_v|/|\langle M_+\rangle_{v,\Delta v=0}|$, and (c) $|\langle M_+^{(1,c)}\rangle_v|/|\langle M_+\rangle_{v,\Delta v=0}|$ as functions of $\gamma G_1 \delta_1$ with the tube position displaced by z_0 from the center of the voxel. The lines in (b) are calculated from Eq. (30a) using continuous values of g_1. The volume ratio of the tube is $\Delta v/v = 0.003$. The frequency shift of the tube is $c = 0.36$ ppm (γB_0). Other parameters used are: $\phi_1 = 0$, $\tau_1 = 10$ ms, $\tau_2 = 2\tau_1$ and number of grid points=$128 \times 128 \times 256$.

insignificant when compared with that of the gradient field. As a result, $\langle M_+\rangle_v \to \langle M_+\rangle_{v,\Delta v=0}$ as if the perturbed field is absent.

In Fig. 4, a dip is found in $|\langle M_+\rangle_v|/|\langle M_+\rangle_{v,\Delta v=0}|$ as the modulation wave vector is varied. The position of the dip occurs at a smaller $\gamma G_1 \delta_1$ and the depth of the dip increases when the size of the tube increases. The relative depth of the dip is defined by

$$\text{relative dip depth} = \frac{|\langle M_+\rangle_{v,\Delta v=0}| - |\langle M_+\rangle_{v,\mathrm{dip}}|}{|\langle M_+\rangle_{v,\mathrm{dip}}|}. \tag{34}$$

Fig. 5a shows the plot of the correlation length that corresponds to the dip position $d_{c,\mathrm{dip}} = \pi/(\gamma G_{1,\mathrm{dip}} \delta_1)$ against the tube width (a_z) for $\tau_2 = 2\tau_1$ and various frequency shifts (c). The plot of the relative depth of the dip against the tube volume ratio ($\Delta v/v$) is shown in Fig. 5b. It should be noted that when $\Delta v/v$ is too large, the dip occurs at a modulation wave vector ($\gamma G_1 \delta_1$) that is too small to be determined accurately from the signal. Therefore only the calculated values with $\Delta v/v \leqslant 2.4\%$ are shown.

Fig. 5a shows that the dip occurs at a correlation length proportional to the characteristic length of the field variation, i.e., $d_{c,\mathrm{dip}} \sim R a_z$ with $1.42 \leqslant R \leqslant 1.86$. On the other hand, Fig. 5b shows that the dip depth increases linearly with $\Delta v/v$ for the range of $\Delta v/v$ under consideration. Both the proportionality constants of the dip position and dip depth are functions of the frequency shift c. For the dip position, it is noted that the minimum of the sinc function in Eq. (30a) occurs at the correlation length of $d_c = 2\pi a_z/4.494 = 1.40 a_z$, which is independent of c. The variation of the dip position for different c thus comes entirely from the third term of Eq. (29). In contrast, for the dip amplitude, both the second and third terms of Eq. (29) contribute to its change when the frequency shift c is varied.

Due to the dependence of the proportionality constants on the frequency shift c as shown in Fig. 5, the acquired correlation length and depth at the signal dip imply a range of characteristic lengths for the field variation. For example, when a dip occurs at $d_{c,\mathrm{dip}} = 0.1 l_z$, the estimated tube width varies from 5.4% to 7.1% of l_z (Fig. 5a). Likewise, when the tube volume ratio is $\Delta v/v = 2.4\%$, the dip depth varies from 1.4% to 5.6% (Fig. 5b). Although Fig. 5 is calculated at the refocusing time of the pulse sequence, there are variations in the signal dip position and dip depth even for the same tube width and volume ratio due to the phase induced by the perturbed field.

The dephasing effect of the gradient field is now examined by shifting the tube with a distance of $z_0 \neq 0$ from the center of the voxel. The normalized total transverse magnetization is plotted against $\gamma G_1 \delta_1$ in Fig. 6a. In the figure, there are rapid oscillations in the signal amplitude as the correlation length is varied when $z_0 \neq 0$. The contributions of the second and third terms of Eq. (29) to the signals in Fig. 6a are plotted separately in Fig. 6b and c. By examining Fig. 6a with the help of Fig. 6b and c, it is seen that the oscillations in the signal amplitude primarily come from $|\langle M_+^{(1,b)}\rangle_v|/|\langle M_+\rangle_{v,\Delta v=0}|$. Eq. (30a) shows that such oscillations arise from the phase factor $\exp(-4ig_1 z_0)$, which is induced by the gradient fields. In the figures, $|\langle M_+^{(1,c)}\rangle_v|/|\langle M_+\rangle_{v,\Delta v=0}|$ is found to be smaller than $|\langle M_+^{(1,b)}\rangle_v|/|\langle M_+\rangle_{v,\Delta v=0}|$ and increases with $\gamma G_1 \delta_1$. Indeed it has been shown previously from Eq. (30) that, for the single tube configuration, the amplitude of $|\langle M_+^{(1,c)}\rangle_v|/|\langle M_+\rangle_{v,\Delta v=0}|$ approaches that of $|\langle M_+^{(1,b)}\rangle_v|/|\langle M_+\rangle_{v,\Delta v=0}|$ in the regime where the correlation length is much smaller than the characteristic length of the field variation.

To include the dephasing effect of the gradient fields, the local perturbed field is modeled by N_b identical square tubes of uniform frequency shift placed randomly in the voxel (Fig. 2b). The normalized total transverse magnetization for a fixed total tube volume

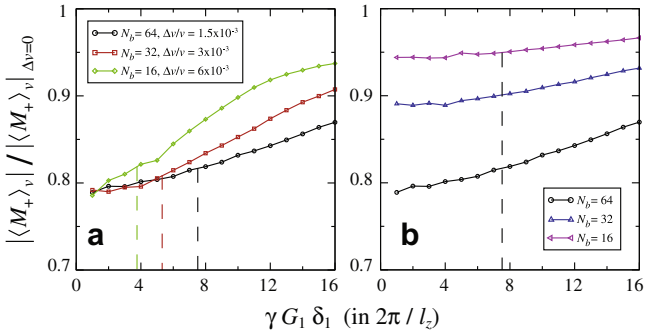

Fig. 7. Plot of $|\langle M_+\rangle_\nu|/|\langle M_+\rangle_{\nu,\Delta\nu=0}|$ as a function of $\gamma G_1\delta_1$ with N_b identical square tubes of uniform frequency shift placed randomly along the x-direction in the voxel (Fig. 2b). (a) The total tube volume ratio is $N_b\Delta\nu/\nu = 0.096$ and the single tube volume ratio is $\Delta\nu/\nu = 1.5\times10^{-3}$, 0.003 and 0.006. (b) The single tube volume ratio is $\Delta\nu/\nu = 1.5\times10^{-3}$ and the total tube volume ratio is $N_b\Delta\nu/\nu = 0.096$, 0.048 and 0.024. The position at which a dip is previously observed is marked according to Fig. 5a. The frequency shift of the tubes is $c = 0.36$ ppm (γB_0). Other parameters used are: $\phi_1 = 0$, $\tau_1 = 10$ ms, $\tau_2 = 2\tau_1$ and number of grid points= $128\times128\times256$.

ratio ($N_b\Delta\nu/\nu = 0.096$) and various single tube volume ratios ($\Delta\nu/\nu$) is plotted against the modulation wave vector $\gamma G_1\delta_1$ in Fig. 7a. In the figure, the modulation wave vector at which a dip was previously observed for the single tube configuration is marked according to Fig. 5a. Since the total volume ratio of the tubes is fixed, the size of each tube, and hence the characteristic length of the local field variation, decreases as N_b increases.

From Fig. 7a, it is seen that the signal feature previously observed at the correlation length around the characteristic length of the local field variation is smoothed out. This can also be seen in Eq. (30a) that, when the signal is averaged over numerous tubes with different z_{0i}, the factor $\exp(-4ig_1z_{0i})$ dephases and the signal dip that reflects the spatial information of the perturbed field diminishes. Nevertheless, it is noted in the figure that the rising rate of the signal depends on the characteristic length of the local field variation. When the modulation wave vector tends to zero or infinity, the DDF signals for the same total tube volume ratio are equal, no matter what the tube sizes are. However, in the intermediate region, the signal rises earlier at a smaller $\gamma G_1\delta_1$ when a larger tube is considered. This rise originates from Eq. (30b) as Eq. (30a) is independent of the gradient field after the averaging over the tube positions. In Fig. 7b, the normalized total transverse magnetization is plotted against $\gamma G_1\delta_1$ for a fixed single tube volume ratio ($\Delta\nu/\nu = 1.5\times10^{-3}$) and various total tube volume ratios. In contrast to Fig. 7a, the rising rates of the signals in Fig. 7b are proportional to the total tube volume ratio. Fig. 7b also shows that the difference of the signal from that of the case with uniform field distribution increases with the total tube volume ratio ($N_b\Delta\nu/\nu$).

To summarize, the results of the block model shows that the rising rate and amplitude of the signal reflect the spatial information of the local field variation, even though the signal dip that occurs at the correlation length around the characteristic length of the field variation becomes insignificant due to the dephasing by the gradient fields.

4.4. Calculations with the blood vessel model

In this subsection, we analyze the dependence of the DDF signal on the correlation length using the blood vessel model. The equilibrium magnetization is again taken to be uniform so that the effect of the field variation on the DDF signal formation is separated from that of the spin density distribution. The susceptibility-induced frequency distribution is now modeled by using N_c infinitely long cylinders of susceptibility difference $\Delta\chi_0$ lying along the x-direction.

Given a general distribution of the susceptibility difference $\Delta\chi(\vec{r})$, the induced frequency distribution can be calculated by [46]

$$\Delta\omega(\vec{r}) = -\frac{\gamma B_0}{3}\int d^3\vec{k}\, e^{i\vec{k}\cdot\vec{r}}\left[3(\hat{k}\cdot\hat{z})^2-1\right]\Delta\tilde{\chi}(\vec{k}) = \frac{\gamma B_0}{2\pi}\int d^3\vec{r}'\, T(\vec{r}-\vec{r}')\Delta\chi(\vec{r}'),$$

with $T(\vec{r}-\vec{r}')$ defined in Eq. (4). For a cylinder lying along the x-direction with radius a_0 and axis located at (y_0,z_0), the susceptibility-induced frequency distribution is [41]

$$\Delta\omega(x,y,z) = \begin{cases} -\frac{\Delta\chi_0}{6}\gamma B_0, & \text{for } (y-y_0)^2+(z-z_0)^2 \leqslant a_0^2, \\ \frac{\Delta\chi_0}{2}\frac{a_0^2}{r_\perp^2}\cos 2\psi\,\gamma B_0, & \text{for } (y-y_0)^2+(z-z_0)^2 > a_0^2, \end{cases} \quad (35)$$

where $r_\perp = \sqrt{(y-y_0)^2+(z-z_0)^2}$ is the perpendicular distance of the point (x,y,z) from the axis of the cylinder and $\psi = \cos^{-1}(\frac{z-z_0}{r_\perp})$ is the azimuthal angle with respect to the axis. Since $\Delta\omega(\vec{r})$ is a convolution of $\Delta\chi(\vec{r})$, the susceptibility-induced frequency distribution for N_c cylinders of susceptibility difference $\Delta\chi_0$ from the background can be constructed by superimposing the induced field of each cylinder using Eq. (35).

In the blood vessel model, the dephasing effects of the gradient field and the perturbed field are entangled. To minimize the dephasing effect of the gradient fields on the signal formation, the cylinder is placed at the center of the voxel (Fig. 2c with $z_0 = 0$). The normalized total transverse magnetization ($|\langle M_+\rangle_\nu|/|\langle M_+\rangle_{\nu,\Delta\nu=0}|$) for various volume ratios of the cylinder ($\Delta\nu/\nu = \pi a_0^2/(l_yl_z)$) are plotted against $\gamma G_1\delta_1$ in Fig. 8a. As shown in the figure, the normalized signal changes more significantly when $\Delta\nu/\nu$ increases. The difference of the signal from that of the uniform case at small $\gamma G_1\delta_1$ increases almost linearly with $\Delta\nu/\nu$ for $\Delta\nu/\nu = 3.75\times10^{-4}$, 7.5×10^{-4}, 1.5×10^{-3}, 3×10^{-3}, 6×10^{-3} and 0.012. The signal for the three smallest volume ratios in Fig. 8a are plotted in an enlarged scale in Fig. 8b. In the plot, a signal dip can be seen as the modulation wave vector is varied. For instance, the dip for $\Delta\nu/\nu = 7.5\times10^{-4}$ (or $a_0 = 0.015l_z$), occurs at a correlation length of about $l_z/8$ to $l_z/4$, which corresponds to a characteristic length scale of the field variation of about 0.067 l_z to 0.176 l_z according to Fig. 5a for the single tube configuration. For a larger $\Delta\nu/\nu$, the dip occurs at a smaller value of $\gamma G_1\delta_1$ (or a larger correlation length), and the dip depth increases. The signal properties observed in the blood vessel model above are similar to those observed in the block model of uniform frequency shift in the last subsection.

The cylinder is now shifted by a distance z_0 from the center of the voxel. The normalized total transverse magnetization ($|\langle M_+\rangle_\nu|/|\langle M_+\rangle_{\nu,\Delta\nu=0}|$) for $\Delta\nu/\nu = 7.5\times10^{-4}$ and different z_0 is plotted against $\gamma G_1\delta_1$ in Fig. 8c. Similar to the signal calculated in Fig. 6a, the signal oscillates as $\gamma G_1\delta_1$ is varied. This signal oscillation comes from the dependence on the phase that is induced by the gradient fields as described in the block model.

To include the dephasing effect of the gradient fields, the local field variation is modeled by randomly placing N_c identical cylinders along the x-direction in the voxel (Fig. 2d). The normalized total transverse magnetizations against $\gamma G_1\delta_1$ for a fixed total cylinder volume ratio ($N_c\Delta\nu/\nu = 0.024$) and for a fixed single cylinder volume ratio ($\Delta\nu/\nu = 3.75\times10^{-4}$) are plotted in Fig. 9a and b, respectively. Similar to the results obtained in the block model, Fig. 9 shows that, despite the smooth out of the signal dip due to the dephasing by the gradient fields, the rising rate and amplitude of the signal depend on the spatial information of the local field variation. In other words, the signal rises earlier at a smaller $\gamma G_1\delta_1$ when a larger cylinder is considered, and the difference of

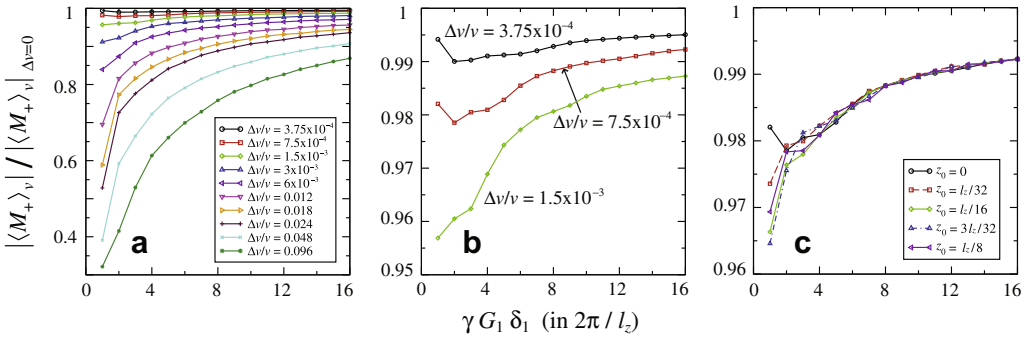

Fig. 8. (a) Plot of the normalized total transverse magnetization $|\langle M_+\rangle_\nu|/|\langle M_+\rangle_{\nu,\Delta\nu=0}|$ as a function of $\gamma G_1\delta_1$ for a cylinder with susceptibility difference $\Delta\chi_0$ for various volume ratios $\Delta\nu/\nu$. The cylinder is placed at the center of the voxel. (b) Plot of the first three volume ratios in (a) in an enlarged scale. (c) Plot of the normalized total transverse magnetization as a function of $\gamma G_1\delta_1$ for $\Delta\nu/\nu = 7.5\times10^{-4}$ and different z_0. Parameters used are: $\Delta\chi_0 = 2.16$ ppm, $\phi_1 = 0$, $\tau_1 = 10$ ms, $\tau_2 = 2\tau_1$ and number of grid points= $128\times128\times128$.

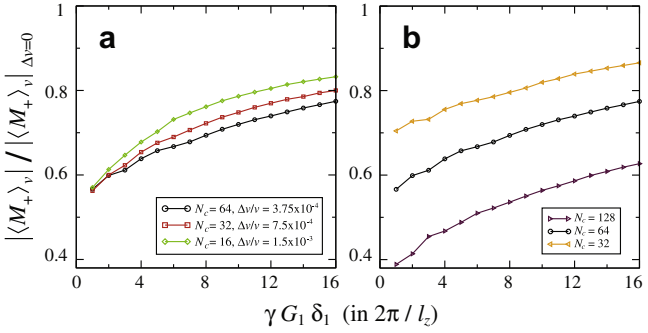

Fig. 9. Plot of $|\langle M_+\rangle_\nu|/|\langle M_+\rangle_{\nu,\Delta\nu=0}|$ as a function of $\gamma G_1\delta_1$ with N_c identical cylinders of susceptibility difference $\Delta\chi_0$ placed randomly along the x-direction in the voxel. (a) The total cylinder volume ratio is $N_c\Delta\nu/\nu = 0.024$ and the single cylinder volume ratio is $\Delta\nu/\nu = 3.75\times10^{-4}$, 7.5×10^{-4} and 1.5×10^{-3}. (b) The single cylinder volume ratio is $\Delta\nu/\nu = 3.75\times10^{-4}$ and the total cylinder volume ratio is $N_c\Delta\nu/\nu = 0.048$, 0.024 and 0.012. Other parameters used are: $\Delta\chi_0 = 2.16$ ppm, $\phi_1 = 0$, $\tau_1 = 10$ ms, $\tau_2 = 2\tau_1$ and number of grid points= $128\times128\times128$.

the signal from that of the case with uniform field distribution increases with the total cylinder volume ratio ($N_c\Delta\nu/\nu$).

5. Conclusions

The distant dipolar field (DDF) signal for a system with a susceptibility-induced local field is studied analytically and numerically using the CRAZED sequence. By examining the integral form of the Bloch equation, it is demonstrated that, after a $\pi/2$ pulse is applied to a system in equilibrium with the static field, there is no odd order of the DDF effect in the transverse magnetization and no even order of the DDF effect in the longitudinal magnetization. Moreover it is shown that when the local field distribution is uniform, the dipolar field has no effect on the evolution of the magnetization after the $\pi/2$ pulse even when the spin density distribution is inhomogeneous. This result justifies the practice of ignoring the DDF effect for the magnetization during the first evolution period of the CRAZED sequence. The analysis of the integral form of the Bloch equation also predicts the dependence of any order DDF approximation of the transverse magnetization on the phase of the first rf pulse of the CRAZED sequence in the presence of a local field distribution. This will be useful to the design of the pulse sequence for the acquisition of a particular order of the DDF signal.

The first order DDF solution is applied to understand the dependence of the DDF signal on the correlation length in the presence of a sub-voxel local field variation. A block model with the field variations modeled by rectangular blocks of uniform resonance frequency shift is developed to manifest the dephasing effects of the perturbed field and the gradient field on the DDF signal formation. Numerical calculations using a single tube of uniform frequency shift are carried out. The results show that a dip appears in the DDF signal when the correlation length is comparable to the width of the tube, provided that the dephasing effect of the gradient fields is suppressed. The dip is found to occur at a correlation length proportional to the tube width, and the dip depth is found to increase with the tube volume ratio. However, it is noticed that the position and depth of the dip are sensitive to the phase induced by the perturbed field during the evolution periods, even when the DDF signal is obtained at the refocusing time. More importantly, the dip is smoothed out when the signal dephasing by the gradient fields is considered. This is demonstrated by randomly placing identical tubes with the same frequency shift in the voxel.

Corresponding numerical calculations are then performed with the field variations constructed by the susceptibility-induced field of infinitely long cylinders placed perpendicular to the static field to mimic the local field induced by blood vessels. The signal characteristics found using the block model are also observed in the blood vessel model.

Although the signal dip that reflects the sub-voxel length scale of the susceptibility-induced field variation is smoothed out when the signal dephasing by the gradient fields is taken into account, both the block model and the blood vessel model show that the DDF signal rises earlier at a smaller modulation wave vector when the spatial length scale of the variations of the local perturbed field is larger. Also the difference of the DDF signal from that of the case with uniform field distribution increases with the volume ratio of the perturbed field region.

For realistic sub-voxel field variations, such as the susceptibility-induced field of numerous blood vessels with various length scales oriented arbitrarily along different directions, the signal dips that reflect the sub-voxel length scales of the susceptibility-induced field variations are expected to be insignificant to be observed due to the dephasing by the gradient fields. As the DDF signal does not show significant qualitative characteristic for different structural length scales, it is not apparent that, by varying the correlation length, the DDF signal can be used directly to reveal a particular length scale of the sub-voxel field variation. Nevertheless, the length scales of the local field variations may be assessed by calculating the Patterson function from the DDF signal, for which further works are needed to be done.

Acknowledgments

The author would like to thank Dr. Kam Wai Clifford Chan for his comments on this paper. Special thanks are given to

Prof. Jianhui Zhong and Prof. Scott D. Kennedy for discussions and introducing the author about the problems on susceptibility-induced field.

Appendix A. Error estimation of the linear DDF approximation

In the numerical calculations of this paper, focus is made on the transverse magnetization with the phase factors $e^{\pm 2i\phi_1}$. We estimate the truncation error in the linear dipolar field approximation of the transverse magnetization that contains the phase factors $e^{\pm 2i\phi_1}$ at the end of the CRAZED sequence.

The terms on the right hand side of Eq. (7) that undergo n dipolar field interactions have amplitude approximately proportional to $(\gamma\mu_0 M_0 t)^n/n!$ relative to the full magnetization for $t \ll T_2$, where M_0 is the equilibrium magnetization. Thus the linear dipolar field term of the transverse magnetization that contains the phase factors $e^{\pm 2i\phi_1}$ at the end of the CRAZED sequence is approximately proportional to $(\gamma\mu_0 M_0\tau_2)$ relative to the full magnetization (see Table 1), whereas the third order term that contains the phase factors $e^{\pm 2i\phi_1}$ is approximately proportional to the sum of $(\gamma\mu_0 M_0\tau_2)^3/6$ and $(\gamma\mu_0 M_0\tau_1)^2(\gamma\mu_0 M_0\tau_2)/2$. The truncation error of keeping the transverse magnetization that is linear in the distant dipolar field is in the order of about $(\gamma\mu_0 M_0\tau_2)^2/6 + (\gamma\mu_0 M_0\tau_1)^2/2$, which is about 2% for a pulse sequence with $\tau_1 = 10$ ms, $\tau_2 = 40$ ms and the parameters for brain at $B_0 = 9.4$ T (cf. Section 4). Therefore the first order dipolar field approximation can be made for the DDF signal formed in the CRAZED sequence without causing severe truncation error.

Appendix B. The uniform block model for susceptibility-induced field distribution

In this Appendix, the results for the block model are derived. A configuration similar to the block model presented here has been used previously to study simulated images formed from the DDF signal [15,16]. These works solved the Bloch equation numerically and showed that there is a decrease in the DDF signal at the boundaries of the blocks of field inhomogeneities, which suggests a new contrast based on the correlation length. In our case, the total transverse magnetization over one voxel of the sample is calculated. We obtain an analytic expression for the magnetization that manifests separately the dephasing effects of the perturbed field and the gradient field on the DDF signal formation. The block model will give insights on how the DDF signal depends on the correlation length in the presence of a sub-voxel field variation and how well the tuning of the correlation distance of the DDF signal reflects the length scale of such variation.

B.1. Samples with periodic sub-voxel structures

In practical situations, MRI often involves imaging of bulk tissues. To calculate the DDF signal of a voxel, the distributions of the equilibrium magnetization and the susceptibility-induced field both inside and outside the voxel have to be specified. This requires a large number of grid points for numerical calculations, and hence tremendous amounts of computational memory and time are needed. Moreover any system used in numerical simulation is finite. A finite system mathematically presumes a periodic boundary condition that the whole system repeats itself beyond the system boundary when discrete Fourier transformation is utilized. These considerations thus suggest the use of a system with periodic structures for further analysis.

The system is taken to be composed of unit cells arranged periodically as shown in Fig. B.1. The size of a unit cell is $l_x \times l_y \times l_z$. Each of these unit cells is used to model a voxel in which the total transverse magnetization is evaluated. Under the periodic boundary assumption, the equilibrium magnetization M_0 and the susceptibility-induced frequency distribution $\Delta\omega$ are periodic functions, viz.,

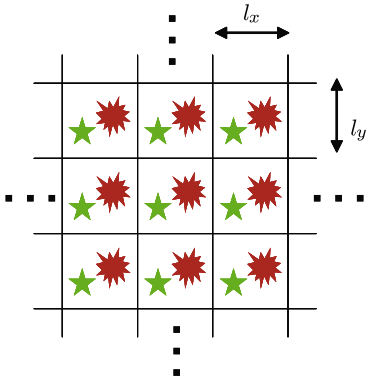

Fig. B.1. Sketch of the unit cells under periodic boundary condition. Each of these unit cells is used to model a voxel in which the total transverse magnetization is evaluated.

$$M_0(\vec{r}) = M_0(\vec{r} + n_x l_x\hat{x} + n_y l_y\hat{y} + n_z l_z\hat{z}), \tag{B.1a}$$

$$\Delta\omega(\vec{r}) = \Delta\omega(\vec{r} + n_x l_x\hat{x} + n_y l_y\hat{y} + n_z l_z\hat{z}), \tag{B.1b}$$

where $\{n_x, n_y, n_z\}$ are integers and $\vec{r} = x\hat{x} + y\hat{y} + z\hat{z}$ with

$$x \in [-l_x/2, l_x/2], \quad y \in [-l_y/2, l_y/2], \quad z \in [-l_z/2, l_z/2]. \tag{B.2}$$

Under the conditions given by Eq. (B.1), the susceptibility-modulated magnetization $\mathscr{M}(\vec{r}, t)$ defined in Eq. (23) is also a periodic function of position $\vec{r}$.

Because of the periodicity, the wave vector $\vec{k}$ introduced in the Fourier transform of the susceptibility-modulated magnetization now takes only discrete values, and the Fourier transform of the susceptibility-modulated magnetization is modified accordingly.

The susceptibility-modulated magnetization within a unit cell ($\mathscr{M}_v$) is defined as

$$\mathscr{M}_v(\vec{r}, t) \equiv M_0(\vec{r})e^{i\Delta\omega(\vec{r})t}. \tag{B.3}$$

It has the same form as $\mathscr{M}(\vec{r}, t)$ in Eq. (23), except now $\vec{r}$ is confined in the domain as given in Eq. (B.2). Now $\mathscr{M}_v$ can be expanded in a Fourier series

$$\mathscr{M}_v(\vec{r}, t) = \sum_{m,p,q=-\infty}^{\infty} \widetilde{\mathscr{M}}_v(\vec{k}_{mpq}, t)e^{i\vec{k}_{mpq}\cdot\vec{r}}, \tag{B.4}$$

where

$$\vec{k}_{mpq} = \left\{\frac{2\pi m}{l_x}, \frac{2\pi p}{l_y}, \frac{2\pi q}{l_z}\right\}, \qquad m, p, q \text{ are integers.} \tag{B.5}$$

The Fourier coefficients are given by

$$\widetilde{\mathscr{M}}_v(\vec{k}_{mpq}, t) = \frac{1}{v}\int_v d^3\vec{r}\,\mathscr{M}_v(\vec{r}, t)e^{-i\vec{k}_{mpq}\cdot\vec{r}}, \tag{B.6}$$

where $\int_v d^3\vec{r}$ denotes the integration over the unit cell volume $v = l_x l_y l_z$. It should be noted that $\widetilde{\mathscr{M}}_v$ is the Fourier transform of the susceptibility-modulated magnetization that is calculated for a finite system in numerical simulation. It is a special case of $\widetilde{\mathscr{M}}$ when periodic structures and discrete $\vec{k}$ values are used. Under the periodic boundary condition, the Fourier transform of the susceptibility-modulated magnetization becomes

$$\widetilde{\mathscr{M}}(\vec{k}, t) = \sum_{m,p,q=-\infty}^{\infty} \delta(\vec{k} - \vec{k}_{mpq})\,\widetilde{\mathscr{M}}_v(\vec{k}_{mpq}, t). \tag{B.7}$$

By substituting Eq. (B.7) into Eq. (26), the first order dipolar field approximation of the transverse magnetization under the periodic boundary condition can be easily obtained. Because of the constraint of the discrete $\vec{k}$ values given in Eq. (B.7), the k-space integrals in Eq. (26) now become discrete sums of $\vec{k}$. Since we are interested in the summed signal of a voxel, the expressions for Eq. (26) with discrete $\vec{k}$ are not written out explicitly here.

B.2. Total transverse magnetization of a unit cell

The integral of a function $f(\vec{r},t)$ over the unit cell volume is denoted by $\langle f(t)\rangle_v \equiv \int_v d^3\vec{r}\, f(\vec{r},t)$. Then, according to Eq. (20), the total transverse magnetization of the unit cell can be written as $\langle M_+\rangle_v = \langle M_+^{(0)}\rangle_v + \langle M_{+,\mathrm{res}}^{(1)}\rangle_v + \langle M_{+,\mathrm{DDF}}^{(1)}\rangle_v$, where $\langle M_+^{(0)}\rangle_v$ is the total transverse magnetization of the unit cell in the zeroth order of the dipolar field, and $\langle M_{+,\mathrm{res}}^{(1)}\rangle_v$ and $\langle M_{+,\mathrm{DDF}}^{(1)}\rangle_v$ are the total transverse magnetizations of the unit cell in the first order of the dipolar field arising, respectively, during the first and second evolution periods of the CRAZED sequence.

From Eq. (21), the total transverse magnetization in the zeroth order of the dipolar field at the end of the CRAZED sequence is found to be

$$\langle M_+^{(0)}(\tau_1+\tau_2)\rangle_v = i\,v e^{-\frac{\tau_1+\tau_2}{T_2}}\left[\cos^2\frac{\theta_2}{2}e^{i\phi_1}\widetilde{\mathscr{M}}_v(\vec{g}_2+\vec{g}_1,-\tau_2-\tau_1) - \sin^2\frac{\theta_2}{2}e^{-i\phi_1}\widetilde{\mathscr{M}}_v(\vec{g}_2-\vec{g}_1,-\tau_2+\tau_1)\right]. \tag{B.8}$$

Here $\vec{g}_1=\gamma\vec{G}_1\delta_1$ and $\vec{g}_2=\gamma\vec{G}_2\delta_2$ are the modulation wave vectors induced by the gradient fields. The periodic condition assumed in the distributions of the equilibrium magnetization and the susceptibility-induced frequency in Eq. (B.1) does not require the gradient field to induce a spatial modulation in the magnetization with an integral number of period across the unit cell. Yet when the modulation wave vectors induced by the gradient fields ($\vec{g}_i$) are integral multiples of the inverse of the unit cell period, i.e.,

$$\vec{g}_i = \left\{\frac{2\pi}{l_x}m,\frac{2\pi}{l_y}p,\frac{2\pi}{l_z}q\right\}, \tag{B.9}$$

where $\{m,p,q\}$ are integers and $i=1,2$ denote the indices of the first and second gradient fields, the resultant wave vector ($\vec{h}$) of any additive or subtractive combination of $\{\vec{g}_1,\vec{g}_2\}$ also gives a spatial modulation with an integral number of period across the unit cell. This condition allows us to simplify the expression of the DDF signal by focusing only on the diffraction peak of the signal:

$$\begin{aligned}\langle M_0(\vec{r})\,e^{i\vec{h}\cdot\vec{r}}\,e^{i\Delta\omega(\vec{r})t}\rangle_v &= v\sum_{m',p',q'=-\infty}^{\infty}\widetilde{\mathscr{M}}_v(\vec{k}_{m'p'q'},t)\,\mathrm{sinc}\,(m'\pi+\frac{h_xl_x}{2})\\ &\quad\times\mathrm{sinc}\,(p'\pi+\frac{h_yl_y}{2})\,\mathrm{sinc}\,(q'\pi+\frac{h_zl_z}{2})\\ &= v\,\widetilde{\mathscr{M}}_v(-\vec{h},t),\quad \text{for}\quad \vec{h}=\left\{\frac{2\pi}{l_x}m,\frac{2\pi}{l_y}p,\frac{2\pi}{l_z}q\right\}.\end{aligned} \tag{B.10}$$

It should be noted that due to the periodic boundary condition, the correlation length induced by the gradient field under Condition (B.9) is much smaller than the sample size, but can be comparable to the sizes of the sub-voxel structures.

From now on, the modulation wave vectors of the gradient fields are taken to be integral multiples of the inverse of the unit cell period. By using Eqs. (26), (B.7) and (B.10), the total transverse magnetization of the unit cell in the first order of the DDF is given by

$$\begin{aligned}\langle M_{+,\mathrm{res}}^{(1)}(\tau_1+\tau_2)\rangle_v &= \frac{1}{2}A_{\theta_2}\,v e^{-\frac{\tau_2}{T_2}}\int_0^{\tau_1}dt'\,e^{-\frac{2t'}{T_2}}\sum_{m,p,q=-\infty}^{\infty}\widetilde{T}(\vec{k}_{mpq})\\ &\quad\times\left[\widetilde{\mathscr{M}}_v(\vec{k}_{mpq},t')\widetilde{\mathscr{M}}_v(-\vec{k}_{mpq}+\vec{g}_2,-t'-\tau_2)\right.\\ &\quad\left.-\widetilde{\mathscr{M}}_v(\vec{k}_{mpq},-t')\widetilde{\mathscr{M}}_v(-\vec{k}_{mpq}+\vec{g}_2,t'-\tau_2)\right]\end{aligned} \tag{B.11a}$$

and

$$\begin{aligned}\langle M_{+,\mathrm{DDF}}^{(1)}(\tau_1+\tau_2)\rangle_v &= -A_{\theta_2}\,v\tau_2\,e^{-\frac{2\tau_1+\tau_2}{T_2}}\sum_{m,p,q=-\infty}^{\infty}\widetilde{T}(\vec{k}_{mpq})\\ &\quad\times\left[e^{i\phi_1}\widetilde{\mathscr{M}}_v(\vec{k}_{mpq}+\vec{g}_1,-\tau_1)+e^{-i\phi_1}\widetilde{\mathscr{M}}_v(\vec{k}_{mpq}-\vec{g}_1,\tau_1)\right]\\ &\quad\times\left[\cos^2\frac{\theta_2}{2}e^{i\phi_1}\widetilde{\mathscr{M}}_v(-\vec{k}_{mpq}+\vec{g}_2+\vec{g}_1,-\tau_2-\tau_1)\right.\\ &\quad\left.-\sin^2\frac{\theta_2}{2}e^{-i\phi_1}\widetilde{\mathscr{M}}_v(-\vec{k}_{mpq}+\vec{g}_2-\vec{g}_1,-\tau_2+\tau_1)\right]\\ &\quad-\frac{1}{2}A_{\theta_2}\,v e^{-\frac{2\tau_1+\tau_2}{T_2}}\int_{\tau_1}^{\tau_1+\tau_2}dt'\sum_{m,p,q=-\infty}^{\infty}\widetilde{T}(\vec{k}_{mpq})\\ &\quad\times\left[e^{i\phi_1}\widetilde{\mathscr{M}}_v(-\vec{k}_{mpq}+\vec{g}_1,t'-\tau_2-2\tau_1)\right.\\ &\quad\left.+e^{-i\phi_1}\widetilde{\mathscr{M}}_v(-\vec{k}_{mpq}-\vec{g}_1,t'-\tau_2)\right]\\ &\quad\times\left[\cos^2\frac{\theta_2}{2}e^{i\phi_1}\widetilde{\mathscr{M}}_v(\vec{k}_{mpq}+\vec{g}_2+\vec{g}_1,-t')\right.\\ &\quad\left.-\sin^2\frac{\theta_2}{2}e^{-i\phi_1}\widetilde{\mathscr{M}}_v(\vec{k}_{mpq}+\vec{g}_2-\vec{g}_1,-t'+2\tau_1)\right].\end{aligned} \tag{B.11b}$$

It is remarked that the dependence of the DDF signal on the local field variation ($\Delta\omega(\vec{r})$) is manifested through the phase of the susceptibility-modulated magnetization, while its dependence on the local spin density variation ($M_0(\vec{r})$) is exhibited more directly through the amplitude of the susceptibility-modulated magnetization.

B.3. Field variations modeled by blocks of uniform frequency shift

To proceed, the equilibrium magnetization is taken to be independent of position $\vec{r}$ to separate the effect of the field variation from that of the spin density distribution. The perturbed field, on the other hand, is modeled by a distribution of rectangular blocks with uniform frequency shifts from the background medium (the block model) as shown in Fig. B.2. In other words, the perturbed field is "digitized" by blocks of different resonance frequencies.

The magnetic field variation in the unit cell is taken to be made up of N_b blocks of uniform frequency shifts. The dimensions of the ith block are taken as $a_{xi}\times a_{yi}\times a_{zi}$, where $i=1,\cdots,N_b$. The domain

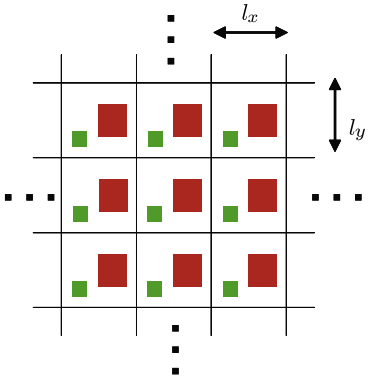

Fig. B.2. Sketch of the unit cells under periodic boundary condition with blocks of uniform frequency shifts from the background medium.

of the ith block with the center located at position $\vec{r}_{0i} = \{x_{0i}, y_{0i}, z_{0i}\}$ is defined by

inside the ith block:

$$|x - x_{0i}| \leqslant \frac{a_{xi}}{2}, \text{ and } |y - y_{0i}| \leqslant \frac{a_{yi}}{2}, \text{ and } |z - z_{0i}| \leqslant \frac{a_{zi}}{2},$$

outside the ith block:

$$|x - x_{0i}| > \frac{a_{xi}}{2}, \text{ or } |y - y_{0i}| > \frac{a_{yi}}{2}, \text{ or } |z - z_{0i}| > \frac{a_{zi}}{2}. \tag{B.12}$$

With c_i taken as the uniform frequency shift of the ith block from the background resonance frequency, the susceptibility-induced frequency distribution can be written as

$$\Delta\omega(\vec{r}) = \begin{cases} c_i, & \text{inside the } i\text{th block}, \\ 0, & \text{outside the blocks}. \end{cases} \tag{B.13}$$

When the equilibrium magnetization is uniform, the susceptibility-modulated magnetization becomes

$$\mathscr{M}_v(\vec{r}, t) = \begin{cases} M_0 e^{ic_i t}, & \text{inside the } i\text{th block}, \\ M_0, & \text{outside the blocks}. \end{cases} \tag{B.14}$$

By using Eq. (B.6), the Fourier component of the susceptibility-modulated magnetization for the block model reads as

$$\widetilde{\mathscr{M}}_v(\vec{k}_{mpq}, t) = M_0 \left[\delta_{\vec{k}_{mpq},\vec{0}} + \sum_{i=1}^{N_b} \frac{\Delta v_i}{v} \left(e^{ic_i t} - 1\right) F_i(\vec{k}_{mpq}) \right], \tag{B.15}$$

where $\{m, p, q\}$ are integers, $\delta_{\vec{k}_{mpq},\vec{0}} = \delta_{m,0}\delta_{p,0}\delta_{q,0}$ is the Kronecker delta function with $\vec{k}_{mpq}$ defined in Eq. (B.5), $\Delta v_i = a_{xi} a_{yi} a_{zi}$ is the volume of the ith block, and

$$F_i(\vec{k}_{mpq}) = e^{-i\vec{k}_{mpq}\cdot\vec{r}_{0i}} \operatorname{sinc}\left(\frac{m\pi a_{xi}}{l_x}\right) \operatorname{sinc}\left(\frac{p\pi a_{yi}}{l_y}\right) \operatorname{sinc}\left(\frac{q\pi a_{zi}}{l_z}\right) \tag{B.16}$$

is a structure-dependent function, which contains the spatial information of the ith block that gives the local perturbed field. It should be noted from Eq. (B.15) that when there is a local field variation, the difference of the susceptibility-modulated magnetization from the equilibrium magnetization is a sum of the structure-dependent function F_i weighted by the volume ratios of the blocks ($\Delta v_i / v$) and the temporal modulation factor ($e^{ic_i t} - 1$), which frequency is determined by the amplitude of the local magnetic field.

By substituting Eq. (B.15) into Eq. (B.11) and using the property of $\widetilde{T}(\vec{k})$ in Eq. (6) for a pair of aligned field gradients (i.e., $\widehat{G}_2 = \widehat{G}_1$ or $-\widehat{G}_1$), the DDF signal of a voxel with phase factors $e^{\pm 2i\phi_1}$ can be expressed in terms of different explicit orders of $\Delta v / v$ as

$$\langle M^{(1)}_{+,2\phi_1} \rangle_v = \langle M^{(1,a)}_{+} \rangle_v + \langle M^{(1,b)}_{+} \rangle_v + \langle M^{(1,c)}_{+} \rangle_v. \tag{B.17}$$

The first term $\langle M^{(1,a)}_{+} \rangle_v$ of Eq. (B.17) does not depend on the ratio $\Delta v_i / v$. It corresponds to the DDF signal formed as if there is no local field variation. The explicit expressions of the three terms in Eq. (B.17) are given by

$$\langle M^{(1,a)}_{+}(\tau_1 + \tau_2) \rangle_v = -3v C_{\theta_2}(\tau_1, \tau_2) \widetilde{T}(\vec{g}_1) \times \left[\cos^2 \frac{\theta_2}{2} e^{2i\phi_1} \delta_{\vec{g}_2 + 2\vec{g}_1, \vec{0}} - \sin^2 \frac{\theta_2}{2} e^{-2i\phi_1} \delta_{\vec{g}_2 - 2\vec{g}_1, \vec{0}} \right], \tag{B.18a}$$

$$\langle M^{(1,b)}_{+}(\tau_1 + \tau_2) \rangle_v = -v C_{\theta_2}(\tau_1, \tau_2) \widetilde{T}(\vec{g}_1) \sum_{i=1}^{N_b} \frac{\Delta v_i}{v} \left[\cos^2 \frac{\theta_2}{2} e^{2i\phi_1} F_i(\vec{g}_2 + 2\vec{g}_1) h_{a,i}(\tau_1, \tau_2) - \sin^2 \frac{\theta_2}{2} e^{-2i\phi_1} F_i(\vec{g}_2 - 2\vec{g}_1) h_{a,i}(-\tau_1, \tau_2) \right], \tag{B.18b}$$

$$\langle M^{(1,c)}_{+}(\tau_1 + \tau_2) \rangle_v = -v C_{\theta_2}(\tau_1, \tau_2) \sum_{m,p,q=-\infty}^{\infty} \widetilde{T}(\vec{k}_{mpq}) \sum_{i=1}^{N_b} \sum_{j=1}^{N_b} \frac{\Delta v_i \Delta v_j}{v^2} \times \left[\cos^2 \frac{\theta_2}{2} e^{2i\phi_1} h_{b,ij}(\tau_1, \tau_2) F_i(\vec{k}_{mpq} + \vec{g}_1) F_j(-\vec{k}_{mpq} + \vec{g}_2 + \vec{g}_1) - \sin^2 \frac{\theta_2}{2} e^{-2i\phi_1} h_{b,ij}(-\tau_1, \tau_2) F_i(\vec{k}_{mpq} - \vec{g}_1) F_j(-\vec{k}_{mpq} + \vec{g}_2 - \vec{g}_1) \right], \tag{B.18c}$$

where $C_{\theta_2}(\tau_1, \tau_2) = \pi^2 \sin\theta_2 \gamma \mu_0 M_0^2 \tau_2 e^{-\frac{\tau_2 + 2\tau_1}{T_2}}$ and

$$h_{a,i}(\tau_1, \tau_2) = -6 + 2e^{-\frac{i}{2}c_i(\tau_2 + 2\tau_1)} \left[2\cos\frac{c_i\tau_2}{2} + \operatorname{sinc}\frac{c_i\tau_2}{2} \right], \tag{B.19a}$$

$$h_{b,ij}(\tau_1, \tau_2) = 3 + 2e^{-i(c_i + c_j)\tau_1} e^{-ic_j\tau_2} - 2e^{-ic_j(\tau_2 + \tau_1)} - 2e^{-ic_i\tau_1} - e^{-\frac{i}{2}c_j(\tau_2 + 2\tau_1)} \operatorname{sinc}\frac{c_j\tau_2}{2} - e^{-\frac{i}{2}c_i(\tau_2 + 2\tau_1)} \operatorname{sinc}\frac{c_i\tau_2}{2} + e^{-\frac{i}{2}(c_i + c_j)(\tau_2 + 2\tau_1)} \operatorname{sinc}\frac{(c_j - c_i)\tau_2}{2}. \tag{B.19b}$$

It is remarked in Eq. (B.18) that the signs of the modulation wave vector induced by the first gradient field ($\vec{g}_1$), the first evolution period (τ_1) and the phase of the first rf pulse (ϕ_1) in the sine terms are opposite to those in the cosine terms. Such dependence originates from Eq. (19) when the phase of part of the transverse magnetization is inverted, i.e., $\alpha(\vec{r}) \to -\alpha(\vec{r})$, right after the second rf pulse.

Eq. (B.18) shows that, with the field variation modeled by blocks of uniform frequency shifts, the DDF signal depends on the phase induced by the gradient field as well as the correlation length and the spatial information of the perturbed field through the structure-dependent function F_i. Also it oscillates in time due to the dependence on the phase induced by the perturbed field through the h functions. When there is only one tube located at the center of the voxel ($\vec{r}_{01} = \vec{0}$), the phase induced by the gradient fields vanishes. In this case, the dephasing effect of the perturbed field on the DDF signal formation can be analyzed separately from that of the gradient field.

In the numerical calculations of this paper, identical tubes of uniform frequency shift lying along the x-direction are considered. The area ratio of the field gradients is taken as $G_2\delta_2 = 2G_1\delta_1$, and the modulation is taken along the z-direction. By putting $a_{xi} = l_x$, $a_{yi} = a_y$, $a_{zi} = a_z$ and $c_i = c$ for the identical tubes, the DDF signal from Eq. (B.17) normalized by that of the case with uniform field distribution can be written as

$$\frac{\langle M^{(1)}_{+,2\phi_1} \rangle_v}{\langle M^{(1)}_{+,2\phi_1} \rangle_{v,\Delta v=0}} = 1 + \frac{\langle M^{(1,b)}_{+} \rangle_v}{\langle M^{(1)}_{+,2\phi_1} \rangle_{v,\Delta v=0}} + \frac{\langle M^{(1,c)}_{+} \rangle_v}{\langle M^{(1)}_{+,2\phi_1} \rangle_{v,\Delta v=0}}, \tag{B.20}$$

with

$$\frac{\langle M^{(1,b)}_{+} \rangle_v}{\langle M^{(1)}_{+,2\phi_1} \rangle_{v,\Delta v=0}} = \frac{\Delta v}{v} \sum_{i=1}^{N_b} \left[h_1(-\tau_1, \tau_2) - \eta e^{-4ig_1 z_{0i}} \operatorname{sinc}(2g_1 a_z) h_1(\tau_1, \tau_2) \right], \tag{B.21a}$$

$$\frac{\langle M^{(1,c)}_{+} \rangle_v}{\langle M^{(1)}_{+,2\phi_1} \rangle_{v,\Delta v=0}} = \frac{\Delta v^2}{v^2} \sum_{i=1}^{N_b} \sum_{j=1}^{N_b} \sum_{p,q=-\infty}^{\infty} \frac{\widetilde{T}(\vec{k}_{0pq} + \vec{g}_1)}{\widetilde{T}(\vec{g}_1)} \times \left\{ h_2(-\tau_1, \tau_2) e^{i\vec{k}_{0pq}\cdot(\vec{r}_{0j} - \vec{r}_{0i})} \operatorname{sinc}^2\left(\frac{p\pi a_y}{l_y}\right) \operatorname{sinc}^2\left(\frac{q\pi a_z}{l_z}\right) - \eta h_2(\tau_1, \tau_2) e^{i(\vec{k}_{0pq} - 2\vec{g}_1)\cdot\vec{r}_{0j}} e^{-i(\vec{k}_{0pq} + 2\vec{g}_1)\cdot\vec{r}_{0i}} \operatorname{sinc}^2\left(\frac{p\pi a_y}{l_y}\right) \times \operatorname{sinc}\left(\frac{q\pi a_z}{l_z} + g_1 a_z\right) \operatorname{sinc}\left(\frac{q\pi a_z}{l_z} - g_1 a_z\right) \right\}, \tag{B.21b}$$

where $\eta = e^{4i\phi_1}\cot^2\frac{\theta_2}{2}$, $g_1 = \gamma G_1 \delta_1$ and

$$h_1(\tau_1,\tau_2) = \frac{2}{3}e^{-\frac{i}{2}c(\tau_2+2\tau_1)}\left[2\cos\frac{c\tau_2}{2} + \operatorname{sinc}\frac{c\tau_2}{2}\right] - 2, \tag{B.22a}$$

$$h_2(\tau_1,\tau_2) = -h_1(\tau_1,\tau_2) + \left[e^{-ic(\tau_2+2\tau_1)} - 1\right]. \tag{B.22b}$$

References

[1] W.S. Warren, W. Richter, A.H. Andreotti, B.T. Farmer II, Generation of impossible cross-peaks between bulk water and biomolecules in solution NMR, Science 262 (1993) 2005–2009.
[2] W. Richter, S. Lee, W.S. Warren, Q. He, Imaging with intermolecular multiple-quantum coherences in solution nuclear magnetic resonance, Science 267 (1995) 654–657.
[3] W.S. Warren, S. Ahn, M. Mescher, M. Garwood, K. Ugurbil, W. Richter, R.R. Rizi, J. Hopkins, J.S. Leigh, MR imaging contrast enhancement based on intermolecular zero quantum coherences, Science 281 (1998) 247–251.
[4] G.D. Charles-Edwards, G.S. Payne, M.O. Leach, A. Bifone, Intermolecular double-quantum coherence imaging of brain tumors at 1.5 T, Proc. Intl. Soc. Mag. Reson. Med. 9 (2001) 922.
[5] R.R. Rizi, S. Ahn, D.C. Alsop, S. Garrett-Roe, M. Mescher, W. Richter, M.D. Schnall, J.S. Leigh, W.S. Warren, Intermolecular zero-quantum coherence imaging of the human brain, Magn. Reson. Med. 43 (2000) 627–632.
[6] J. Zhong, Z. Chen, E. Kwok, In vivo intermolecular double-quantum imaging on a clinical 1.5 T MR scanner, Magn. Reson. Med. 43 (2000) 335–341.
[7] W. Richter, M. Richter, W.S. Warren, H. Merkle, P. Andersen, G. Adriany, K. Ugurbil, Functional magnetic resonance imaging with intermolecular multiplequantum coherences, Magn. Reson. Imag. 18 (2000) 489–494.
[8] J. Zhong, E. Kwok, Z. Chen, fMRI of auditory stimulation with intermolecular double-quantum coherences (iDQCs) at 1.5 T, Magn. Reson. Med. 45 (2001) 356–364.
[9] A. Schäfer, T.H. Jochimsen, H.E. Möller, Functional magnetic resonance imaging with intermolecular double-quantum coherences at 3 T, Magn. Reson. Med. 53 (2005) 1402–1408.
[10] T. Gu, S.D. Kennedy, Z. Chen, J. Zhong, Functional MRI at 3 T using intermolecular double quantum coherence (iDQC) with spin-echo or gradient-echo acquisitions, Magn. Reson. Mater. Phys. 20 (2007) 255–264.
[11] L.S. Bouchard, W.S. Warren, Multiple-quantum vector field imaging by magnetic resonance, J. Magn. Reson. 177 (2005) 9–21.
[12] R. Bowtell, P. Robyr, Structural investigations with the dipolar demagnetizing field in solution NMR, Phys. Rev. Lett. 76 (1996) 4971–4974.
[13] P. Robyr, R. Bowtell, Nuclear magnetic resonance microscopy in liquids using the dipolar field, J. Chem. Phys. 106 (1997) 467–476.
[14] P. Robyr, R. Bowtell, Measuring Patterson functions of inhomogeneous liquids using the nuclear dipolar field, J. Chem. Phys. 107 (1997) 702–706.
[15] T. Enss, S. Ahn, W.S. Warren, Visualizing the dipolar field in solution NMR and MR imaging: three-dimensional structures simulations, Chem. Phys. Lett. 305 (1999) 101–108.
[16] S. Garrett-Roe, W.S. Warren, Numerical studies of intermolecular multiple quantum coherences: high-resolution NMR in inhomogeneous fields and contrast enhancement in MRI, J. Magn. Reson. 146 (2000) 1–13.
[17] R. Bowtell, S. Gutteridge, G. Ramanathan, Imaging long-range dipolar field in structured liquid samples, J. Magn. Reson. 150 (2001) 147–155.
[18] C. Ramanathan, R.W. Bowtell, NMR imaging and structure measurements using the long-range dipolar field in liquids, Phys. Rev. E 66 (2002) 041201.
[19] L.-S. Bouchard, R.R. Rizi, W.S. Warren, Magnetization structure contrast based on intermolecular multiple-quantum coherences, Magn. Reson. Med. 48 (2002) 973–979.
[20] S. Gutteridge, C. Ramananathan, R.W. Bowtell, Microscopic susceptibility contrast in the CRAZED experiment, Proc. Intl. Soc. Mag. Reson. Med. 10 (2002) 615.
[21] J.P. Marques, R. Bowtell, Numerical simulations of the DQC signal in inhomogeneous solutions, Proc. Intl. Soc. Mag. Reson. Med. 11 (2003) 1108.
[22] X.-P. Tang, C.-L. Chin, L.-S. Bouchard, F.W. Wehrli, W.S. Warren, Observing Bragg-like diffraction via multiple coupled nuclear spins, Phys. Lett. A 326 (2004) 114–125.
[23] G.D. Charles-Edwards, G.S. Payne, M.O. Leach, A. Bifone, Effects of residual single-quantum coherences in intermolecular multiple-quantum coherence studies, J. Magn. Reson. 166 (2004) 215–227.
[24] S. Kirsch, P. Bachert, Diffraction-like phenomena in a periodic magnetization distribution at 1.5 T using the distant dipolar field (DDF), J. Magn. Reson. 185 (2007) 183–190.
[25] S. Capuani, F. Curzi, F.M. Alessandri, B. Maraviglia, A. Bifone, Characterization of trabecular bone by dipolar demagnetizing field MRI, Magn. Reson. Med. 46 (2001) 683–689.
[26] S. Capuani, G. Hagberg, F. Fasano, I. Indovina, A. Castriota-Scanderbeg, B. Maraviglia, In vivo multiple spin echoes imaging of trabecular bone on a clinical 1.5 T MR scanner, Magn. Reson. Imag. 20 (2002) 623–629.
[27] C.-L. Chin, X. Tang, L.-S. Bouchard, P.K. Saha, W.S. Warren, F.W. Wehrli, Isolating quantum coherences in structural imaging using intermolecular double-quantum coherence MRI, J. Magn. Reson. 165 (2003) 309–314.
[28] L.-S. Bouchard, F.W. Wehrli, C.-L. Chin, W.S. Warren, Structural anisotropy and internal magnetic fields in trabecular bone: coupling solution and solid dipolar interactions, J. Magn. Reson. 176 (2005) 27–36.
[29] A. Schäfer, H.E. Möller, Functional contrast based on intermolecular double-quantum coherences: influence of the correlation distance, Magn. Reson. Med. 58 (2007) 696–704.
[30] C.K. Wong, Theoretical Studies of the Properties of Magnetic Resonance Signal Formed under the Influence of Distant Dipolar Field, Ph.D. thesis, University of Rochester, 2008.
[31] G. Deville, M. Bernier, J.M. Delrieux, NMR multiple echoes observed in solid ^{3}He, Phys. Rev. B 19 (1979) 5666–5688.
[32] J. Jeener, Collective effects in liquid NMR: dipolar field and radiation damping, in: D.M. Grant, R.K. Harris (Eds.), Encyclopedia of Nuclear Magnetic Resonance, vol. 9, Wiley, New York, 2002, pp. 642–679.
[33] S. Gutteridge, C. Ramanathan, R. Bowtell, Mapping the absolute value of M0 using dipolar field effects, Magn. Reson. Med. 47 (2002) 871–879.
[34] M. Engelsberg, W. Barros Jr., Distant-dipole field in liquids and diffusion: a perturbative approach, J. Chem. Phys. 122 (2005) 034501–034504.
[35] C.K. Wong, S.D. Kennedy, E. Kwok, J. Zhong, Theoretical studies of the effect of the dipolar field in multiple spin-echo sequences with refocusing pulses of finite duration, J. Magn. Reson. 185 (2007) 247–258.
[36] W. Barros Jr., D.F. Gochberg, J.C. Gore, Nuclear magnetic resonance signal dynamics of liquids in the presence of distant dipolar fields, revisited, J. Chem. Phys. 130 (2009) 174506.
[37] C.K. Wong, J. Zhong, Roles of magnetic gradient field and transverse relaxation in distant dipolar field signal, Concepts Magn. Reson. Part A 34A (2009) 76–90.
[38] S.D. Kennedy, Z. Chen, C.K. Wong, E.W.-C. Kwok, J. Zhong, Investigation of multiple-echo spin-echo signal acquisition under distant dipole–dipole interactions, Proc. Intl. Soc. Mag. Reson. Med. 13 (2005) 2288.
[39] X. Tang, H. Ong, K. Shannon, W.S. Warren, Simultaneous acquisition of multiple orders of intermolecular multiplequantum coherence images, Magn. Reson. Imaging 21 (2003) 1141–1149.
[40] E.D. Minot, P.T. Callaghan, N. Kaplan, Multiple echoes, multiple-quantum coherence, and the dipolar field: demonstrating the significance of higher order terms in the equilibrium density matrix, J. Magn. Reson. 140 (1999) 200–205.
[41] E.M. Haacke, R.W. Brown, M.R. Thompson, R. Venkatesan, Magnetic Resonance Imaging: Physical Principles and Sequence Design, Wiley-Liss, New York, 1999.
[42] J.P. Marques, R. Bowtell, Simulations of the BOLD effect using a realistic model of the vasculature, NMR Biomed. 21 (2008) 553–565.
[43] Z. Chen, S. Zheng, J. Zhong, Optimal RF flip angles for multiple spin-echoes and iMQCs of different orders with the CRAZED pulse sequence, Chem. Phys. Lett. 347 (2001) 143–148.
[44] S.-P. Lee, A.C. Silva, K. Ugurbil, S.-G. Kim, Diffusion-weighted spin-echo fMRI at 9.4 T: microvascular/tissue contribution to BOLD signal changes, Magn. Reson. Med. 42 (1999) 919–928.
[45] R.T. Branca, S. Capuani, B. Maraviglia, About the Crazed sequence, Concepts Magn. Reson. Part A 21A (2004) 22–36.
[46] R. Salomir, B. Denis De Senneville, C.T.W. Moonen, A fast calculation method for magnetic field inhomogeneity due to an arbitrary distribution of bulk susceptibility, Concepts Magn. Reson. Part B 19B (2003) 26–34.